Mitochondrial dynamics and autophagy during giant lipid droplet formation in oleaginous yeast

油脂酵母の巨大脂肪滴形成における
ミトコンドリア動態とオートファジー

LAN DUAN
段 瀾

Laboratory of Mitochondrial Dynamics
Graduate School of Frontier Biosciences
Osaka University

December 2024

Abstract

Emerging evidence suggests a pivotal involvement of mitochondria and autophagy in lipid droplet (LD) biogenesis and breakdown. In contrast to the conventional yeasts containing small multiple LDs, the oleaginous yeast *Lipomyces starkeyi* has a remarkable ability to generate a single giant LD, attracting a great deal of attention as an excellent lipid supplier for promoting biofuel production in the chemical industries. Although formation of giant LDs appears to be induced and regulated through mitochondrial metabolism under autophagy-inducing nitrogen starvation, challenges in genetic manipulation have impeded the comprehensive understanding of mitochondrial behavior and autophagy-related processes in this unconventional yeast.

To overcome these issues, I generated an *L. starkeyi* strain expressing mito-DHFR-mCherry, a mitochondrial fluorescent marker, and investigated, for the first time, mitochondrial dynamics under various growth conditions using fluorescence microscopy and western blotting. I found that a fraction of mitochondria was localized to the vacuole, a lytic organelle in yeast, indicating degradation of mitochondria in *L. starkeyi* cells. Next, I generated an *L. starkeyi* strain defective in lipidation of the ubiquitin-like protein LsAtg8, a process required for autophagy, and found that mitochondrial degradation was strongly suppressed, establishing this catabolic event as mitophagy (mitochondrial autophagy). My observation also revealed minimal mitophagy during giant LD formation under nitrogen starvation. Notably, mitochondria transitioned from fragmented to thinned morphology and juxtaposed to giant LDs under nitrogen starvation, whereas they kept fragmented in cells lacking giant LDs under carbon-limited conditions. Surprisingly, *L. starkeyi* cells exhibited suppression or promotion of autophagy under conditions depleting nitrogen or carbon, respectively.

These findings suggest that nitrogen-starved *L. starkeyi* cells undergo formation of giant LD in close proximity to elongated mitochondria in a manner independent of mitophagy and autophagy.

Content

Chapter 1. General Introduction

1-1 Lipid droplets (LDs)

Lipid droplets (LDs), long regarded as fat reservoirs, are highly conserved organelles involved in energy metabolism. LDs are constructed by a central neutral lipid core that is mainly composited with triacylglycerols (TAGs) and sterol esters and surrounded by a single phospholipid layer and proteins [1]. Beyond their function in energy metabolisms through lipid uptake, storage, and distribution, multiple lines of evidence reveal that LDs also play critical roles in cellular protection, organelle integrity, redox homeostasis, membrane maintenance, and autophagy in response to cellular stress or environmental requirements [2-5]. However, many of those functions are engaged simultaneously and cooperate with other organelles, such as the endoplasmic reticulum (ER), peroxisomes, lysosomes, Golgi, and mitochondria [6, 7], making it difficult to study the molecular mechanisms underlying those activities.

1-2 The basis of autophagy

Autophagy is an intracellular degradation and recycling system that is highly conserved among almost all eukaryotes. There are three types of autophagy that have been established so far: microautophagy, macroautophagy and chaperone-mediated autophagy (CMA) (Figure 1-1) [8]. Despite the differences among their mechanisms, they implement the transport and clearance of cellular components in lysosomes. In microautophagy, cargoes are directly captured into lysosomes by invaginations or protrusions of the lysosomal membrane [9]. During macroautophagy, cargoes are sequestrated by double-membrane vesicles, named autophagosomes, and subsequently transported into lysosomes for their degradation. CMA differs from microautophagy and macroautophagy in that cargoes (proteins with pentapeptide motifs) are not captured by membrane structures but targeted by molecular chaperones and translocated directly through the lysosomal membrane [10]. Microautophagy and macroautophagy are conserved among eukaryotes and degrade both organelles and proteins, whereas CMA has so far been found to degrade only proteins in mammals. Among those three types of autophagy, macroautophagy is the most understood and the most universal mechanism. Hereafter, macroautophagy in this thesis is referred to as autophagy.

As described above, autophagy is an intracellular degradation system that generates isolation membranes surrounding intracellular constituents and forms double membrane-bound autophagosomes to sequester and transport the cargoes into lysosomes (or vacuoles in yeast) and degrade them for recycling and remodeling to achieve cellular survival [11]. It has been widely established that autophagy can be induced by nutrient deprivation to non-selectively degrade cellular components [12]. On the other hand, autophagy can also degrade cargoes in a

selective way, such as specific proteins and organelles. To date, cargoes of selective autophagy have extensively been characterized, including vacuolar enzymes (cytoplasm to vacuole targeting (Cvt) pathway), mitochondria (mitophagy), peroxisomes (pexophagy), ER (ER-phagy), nuclei (nucleophagy), lipid droplets (lipophagy) [13-17]. Emerging evidence suggests that autophagy has high potential for the treatment of cancer, Parkinson's disease, melanoma, obesity, diabetes, and aging. However, the underlying mechanisms are still not fully understood [18].

1-3 Molecular mechanisms of autophagy in the yeast *Saccharomyces cerevisiae*

The process of autophagy is categorized into five distinct stages: (1) initiation by pre-autophagosomal structure/phagophore assembly site (PAS) formation, (2) elongation of isolation membrane, (3) enclosure of autophagosomes (maturation), (4) fusion with vacuoles, and (5) degradation in vacuoles. In the yeast *Saccharomyces cerevisiae*, the basic mechanisms of autophagy have been extensively studied. After numerous investigations, more than 40 autophagy-related (Atg) proteins have been identified in yeast, 15 of which function as the core factors for autophagosome formation [19].

The initiation step of autophagy in yeast is regulated by the Atg1 serine/threonine kinase and Atg13, a regulatory subunit, and the Atg17-Atg29-Atg31 complex. Atg1 is the only kinase of the core autophagy machinery whose activity is regulated by PKA-dependent phosphorylation and the target of rapamycin (TOR), and is essential for its PAS localization. Under nutrient-rich conditions, Atg13 is hyperphosphorylated by TOR complex 1 (TORC1) and/or PKA. When the condition is shifted from nutrient-rich to starvation, TORC1 is inactivated, resulting in dephosphorylation of Atg13 to promote Atg1-Atg13 interactions and Atg1 activation. Atg13 dephosphorylation also helps Atg13-Atg17 binding, and subsequent formation of the Atg1-Atg13-Atg17-Atg29-Atg31 complex, which is a prerequisite for PAS formation.

After the Atg1 complex localizes to the PAS, Atg9-containing tubulovesicles are recruited to the PAS for phagophore elongation. Atg9 is a transmembrane protein that localizes to the trans-Golgi network and endosomes or endosome-like structures [20]. When autophagy is induced, Atg9 shuttles between the periphery sites and PAS to transfer small vesicles to the PAS. The forward process depends on Atg11, Atg23 and Atg27, and the backward process relies on binding of Atg9 with Atg1-Atg13 and Atg2-Atg18. Atg9 movement is also mediated by the class III PtdIns3K complex [21].

The class I phosphatidylinositol 3-kinase (PI3K) complex, consisting of Vps34, Vps15, Atg6/Vps30, Atg14 and Atg38, is recruited to PAS after the recruitment of Atg9-containing tubulovesicles [22, 23]. Vps34, the sole PI3K in yeast, forms two distinct complexes, complex I for autophagy and II for protein sorting to vacuoles. The complex I phosphorylates phosphatidylinositol (PI) to generate phosphatidylinositol 3-phosphate (PI3P), which is essential for PAS localization of the PI3P-binding protein Atg18. Subsequently, Atg18 forms a complex with Atg2 and further promotes elongation of the phagophore. The Atg2-Atg18 complex also binds to Atg9, further accelerating transport of lipids from periphery sites to the PAS [24, 25].

In addition, there are two ubiquitin conjugation systems, the Atg12 system and the Atg8 system, required for autophagy promotion. Atg12 is activated by the E1-like activating enzyme Atg7, transferred to E2-like conjugating enzyme Atg10, and covalently linked to Atg5. Atg12–Atg5 interacts with Atg16 and localizes to the PAS in a manner dependent on PI3P and the Atg1 kinase complex. When autophagy is induced, the Atg8 Arg117 residue at its C-terminus is cleaved off by Atg4, a cysteine protease, to expose the Gly116 residue, which is required for its conjugation to phosphatidylethanolamine (PE). After the cleavage of the C-terminus, Atg8 is activated by Atg7, processed by the E2-like conjugating enzyme Atg3, and covalently linked to PE [26, 27]. This process is also called lipidation, helping the elongation of phagophores. Atg4 also acts as a delipidation enzyme to release Atg8 from PE and recycle Atg8 for the other around of lipidation [28].

Most of the core Atg proteins are shared for both non-selective and selective autophagy events, while there are also some Atg proteins that act as receptors to target specific cargoes and initiate selective autophagy for their degradation. For instance, Atg32 for mitophagy, Atg39 and Atg40 for ER-phagy, and Atg36 for pexophagy.

1-4 LD biogenesis

In eukaryotes, LD biogenesis is widely thought to start with the synthesis of lipids (TAGs and steryl esters) between the two leaflets of the ER membrane by the enzymes of neutral lipid synthesis [29-32]. TAG synthesis is catalyzed by two diacylglycerol acyltransferases (DGATs), DGAT1 and DGAT2 [33-35]. Steryl esters are generated by Are1 and Are2, acyl-CoA: sterol acyltransferases in yeast [36] and by ACAT1 and ACAT2, acyl-CoA: cholesterol acyltransferases in mammals [33, 37-39]. As LDs grow larger and mature within the lipid bilayer of the ER membrane, biophysical processes drive lens formation at the ER tubules and then budding from the ER (Figure 1-2) [30].

In general, lipid synthesis and accumulation can be stimulated by excess carbon or the deprivation of other essential nutrients (nitrogen, especially) [40], whereas they are highly suppressed by carbon depletion. Biosynthesis of microbial oils usually requires nitrogen-starvation conditions [41]. It has been reported that nitrogen depletion can induce citric acid (CA) accumulation in oleaginous yeast cells [42]. CA can then be converted to acetyl-CoA by ATP-citrate lyase, serving as a critical feedstock for lipids biosynthesis in oleaginous yeast. Acetyl-CoA is further converted to acyl-CoA (C16, C18) by fatty acid synthases (FAS1, FAS2) [43, 44]. The resulting acyl-CoA (C16, C18) is further transported into the ER, and subsequently contributes to TAG synthesis through the Kennedy pathway [45].

1-5 LD breakdown via lipolysis and lipophagy

LD breakdown occurs through two major mechanisms: lipolysis and lipophagy [46-48], that are essential catabolic pathways activated in response to nutrient deprivation. Lipolysis enables highly regulated release of fatty acids (FAs) from TAGs by the sequential action of lipases [48]. Lipophagy is a recently discovered selective autophagic process by which a portion of or the whole LDs are engulfed within lysosomes (or vacuoles in yeast) for their degradation [49, 50]. Mammalian hepatocytes and macrophages seem to undergo both macroautophagy and microautophagy that transport LDs to lysosomes with or without membrane vesicles containing LC3, a mammalian Atg8 family protein [51-55]. Lipophagy in the yeast *S. cerevisiae* utilizes a microautophagy-like mechanism by which LDs are directly enclosed and degraded by vacuoles (Figure 1-3) [56-61].

1-6 Relationship between LD metabolism and autophagy

Accumulating evidence reveals the regulatory function of autophagy in LD formation. In hepatocytes, LDs are occasionally found inside the autophagosomes. A fraction of neutral lipids colocalizes with autophagosomal or lysosomal proteins, indicating that autophagy is involved in lipid degradation. Moreover, inhibition of autophagy by atg5 knockdown leads to TAG and cholesterol accumulation with exogenous or endogenous lipid stimulus in hepatocytes [62], facilitating LD expansion in both number and size. LD increase can also be induced by inhibition of autophagy, even without lipid stimulus, further suggesting that autophagy acts in LD metabolism. However, inhibition of autophagy in hepatocytes only decreased the level of lipolysis and FA β-oxidation but had no interference with TAG synthesis. Similar mechanisms have also been found in mice: atg7 knock-out in hepatocytes causes enlargement of livers due to a significant increase in the TAG and cholesterol amount.

In addition, an increase in the cellular lipid content leads to suppression of autophagy [62, 63]. Although the basic mechanisms are still not clear, this autophagic dysfunction is possibly due to altered lipid compositions in autophagosomes and defects in fusion between autophagosomes and lysosomes.

The interplay between autophagy and LD formation in yeast is less understood. LD turnover is dependent on microautophagy but not macroautophagy in *S. cerevisiae*: LDs are engulfed by invaginations or protrusions of the vacuolar membrane under nitrogen starvation conditions [59]. Furthermore, cytosolic lipase activity decreases significantly, whereas vacuolar lipase activity increases in nitrogen-starved cells. This intravacuolar catabolic event does not require Atg1 but depends on the vacuolar lipase Atg15. In the absence of Atg1, LDs remain in the cytosol and proceed to cytosolic lipolysis. In the absence of Atg15, LDs accumulate in vacuoles, leading to a decrease in TAG degradation products [64]. Atg15 might also be involved in lipid degradation via the digestion of other membranous organelles, such as mitochondria and peroxisomes, in the vacuole [65, 66]. Additional investigations are required to substantiate this hypothesis.

1-7 Autophagy-unrelated function of Atg8 (or LC3 in mammals) in LD formation

Microtubule-associated protein (MAP) light chain 3 (LC3), a homologue of Atg8, associates with LDs in the absence of a double-membrane structure in both fed and starved mice [62]. In hepatocytes and cardiac myocytes, lipid-conjugated LC3 is required for LD accumulation [67, 68]. In yeast, Atg8 functions in the maintenance of LD quantity in a manner independent of its lipidation system[69]. These findings suggest that Atg8-family proteins may localize on the LD surface and function in LD biogenesis.

1-8 Interactions of LDs with mitochondria and other organelles

Previous studies establish the interactions between LDs and other organelles in multiple cell types. Among those interactions, LD-ER is the most prominent one that has been revealed in mammalian cells [70], yeast [30], and non-yeast cells [71]. LDs are often kept in close contact with the ER for their budding and enzyme migration for LD expansion. They also interact with peroxisomes in yeast (Figure 1-2, 1-3) [72], possibly for FA β-oxidation.

Besides the aforementioned interactions, LD-mitochondria is widely found in various mammalian cells, particularly in skeletal or heart muscl [73-75] and brown adipose tissue (BAT) [76]. Mitochondria function in multiple cellular processes such as ATP production, calcium

signaling, iron homeostasis, FA β-oxidation, and TAG biogenesis [77-79]. Those functions allow them to act in a variety of cellular events, such as apoptosis, innate immune response, and cell differentiation [80, 81]. There are multiple studies suggesting that LD-mitochondria interactions may serve to facilitate transfer of FAs to mitochondria for β-oxidation [82-84] and LD expansion [85].

Mitochondria in close contact with LDs, named PDM (peridroplet mitochondria), are found in mammals, such as rat skeletal muscle [75], mouse heart muscle [73], mouse brown adipose tissue (BAT) [76], and hepatocytes [86], etc. Mitochondria-LD interactions increase under starvation conditions, presumably increasing FA oxidation in mitochondria [82-84]. PDM has a high capacity to oxidize pyruvate and malate, thereby promoting TAG synthesis, whereas it has a low capacity for fat oxidation, compared to cytosolic mitochondria (CM), ultimately resulting in LD expansion [85]. In BAT and immune cells, mitochondria undergo both lipid synthesis and oxidation at the same time [87-89], challenging the conventional concept that mitochondria cannot support both lipid synthesis and oxidation simultaneously [90, 91]. As PDM have bioenergetics, proteome, cristae organization, and dynamics that are distinct from those of CM [92], their functions in LD biogenesis remain largely unexplored.

The yeast *S. cerevisiae* is widely used for studying organelle-organelle contact, especially mitochondrial contacts with the ER [93], vacuoles [94], and peroxisomes [95]. In contrast, the LD-mitochondria contact in yeast remains poorly understood [75, 96]. It is probably because β-oxidation in *S. cerevisiae* primarily occurs in peroxisomes, and acetyl-CoA, a product of β-oxidation in peroxisomes, is transported to mitochondria for generating ATP via the TCA cycle [96].

1-9 Molecular mechanisms of mitophagy in the yeast *Saccharomyces cerevisiae*

Mitochondria function in energy supply through oxidative phosphorylation (OXPHOS). After long-term respiration, reactive oxygen species (ROS), the byproducts of OXPHOS, excessively accumulate to increase oxidative stress that is harmful to mitochondria [97], and eventually induces mitochondrial dysfunction. Consequently, accumulation of damaged mitochondria leads to various diseases such as Alzheimer's disease (AD), Parkinson's disease, immune diseases, cancers, and accelerates aging [98, 99]. Thus, clearance of damaged and excess mitochondria is critical for cellular health.

Mitophagy is an evolutionarily conserved mechanism that selectively captures and encases dysfunctional or excess mitochondria by double membrane-bound autophagosomes and transports them to lysosomes (or vacuoles in yeast) for their degradation (Figure 1-4) [100,

101]. Mitophagy can be classified into two distinct modes, receptor and ubiquitin-mediated processes. In mammalian cells, both mitophagic processes occur, whereas only receptor-mediated mitophagy exists in yeast.

Receptor-mediated mitophagy in the yeast *S. cerevisiae* is strictly dependent on Atg32, a single transmembrane protein that is anchored on the mitochondrial outer membrane[102, 103]. Loss of Atg32 leads to nearly complete inhibition of mitophagy but has no interference with other types of selective and non-selective autophagy. Upon mitophagy initiation, Atg32 Ser114 and Ser119 are phosphorylated, which is essential for its interaction with Atg11, a scaffold protein critical for selective autophagy. Phosphorylation of Atg32 is mediated by casein kinase 2 (CK2 [104]. Conversely, dephosphorylation of Atg32 is mediated by the protein phosphatase 2A (PP2A)-like protein Ppg1 [105]. Loss of Ppg1 leads to Atg32 hyperphosphorylation, resulting in stabilization of Atg32-Atg11 interactions to promote mitophagy.

After phosphorylation, Atg32 interacts with Atg11 and Atg8, forming a ternary complex, which is a prerequisite for mitophagosome formation. Atg11 further recruits Atg1, Atg7, Atg9, and other core Atg proteins, facilitating formation of autophagosomes surrounding mitochondria.

1-10 Mitophagy and mitochondria dynamics during LD biogenesis and breakdown

Mitochondrial degradation by mitochondrial-specific autophagy (mitophagy) is thought to be critical for cellular fat homeostasis [101,106] Recent studies demonstrate that mitophagy is significantly activated in BAT after chronic cold exposure [107], and that it also functions in alleviation of high-fat diet-induced obesity and diabetic cardiomyopathy [108, 109]. DGAT1 (diacylglycerol O-acyltransferase 1) is a protein that functions in LD biogenesis upon iron chelation in various cell types. DGAT1-dependent lipid droplet biosynthesis occurs prior to mitochondrial turnover, with many LDs interacting with mitochondria upon iron chelation [110]. Notably, inhibition of DGAT1 impairs mitophagy. Moreover, deletion of mdy (an ortholog of DGAT1) impairs neuronal mitophagy in *Drosophila*.

Besides mitochondrial degradation, mitochondrial fission and fusion are involved in LD dynamics. In murine brown adipose tissue, defects in mitochondrial fusion with deficiency of Mfn2, a GTPase that mediates mitochondrial outer membrane fusion [111], impair mitochondria by reducing β-oxidation and mitochondrial respiration, promoting LD accumulation and FA efflux from cells [84]. Still, how mitochondrial dynamics and degradation affect or are affected by LD remains unclear (Figure 1-5).

1-11 Lipid droplets in the oleaginous yeast *Lipomyces starkeyi*

Among unicellular eukaryotes, the oleaginous yeast *L. starkeyi* is one of the most attractive organisms that can metabolize a wide variety of carbon and nitrogen sources and accumulate giant LDs above 65% of its dry weight [112], making it a striking candidate for industrial oil production and an ideal yeast model for studying mitochondrial functions in LD metabolism. Lipid accumulation in *L. starkeyi* can be affected by various factors such as the carbon-to-nitrogen ratio, pH, temperature, aeration speed, inoculum age, fermentation time, and inhibitors [40, 113], which results in uncertainty to the final lipid yield. The wild-type *L. starkeyi* NBRC10381 cells can accumulate lipid content up to 85% of their dry weight under nitrogen-limited culture conditions [114]. Even despite the difficulties in genetic manipulations of this unconventional yeast, I have recently succeeded to visualize mitochondria in *L. starkeyi NRRL Y-1388* using mito-DHFR-mCherry, a mitochondrial matrix-targeted red fluorescent marker fused with dihydrofolate reductase, making it a potential yeast model for studying mitochondria and LDs [115].

1-12 The scope of this study

Emerging evidence reveals that LDs are regarded as not only the fat reservoirs, but also metabolism regulators and lipotoxity defenders for protecting membranous organelles. Recent studies in mammalian and yeast models suggest the influence of LD biogenesis and breakdown on mitochondrial dynamics and autophagy, however, their functions and mechanisms are still unclear.

In this thesis, I focused on mitochondrial behavior under different LD formation conditions in the oleaginous yeast *L. starkeyi*. I successfully labeled mitochondria in *L. starkeyi* and developed *L. starkeyi* as a useful model to monitor mitochondrial behavior in giant LD biogenesis. Using this mitochondria-labeled *L. starkeyi* strain, I found that mitochondrial degradation occurs in *L. starkeyi* cells. This catabolic event is strongly suppressed during giant LD formation upon nitrogen starvation. In addition, mitochondrial shape transitioned to thinned morphology, in close proximity to LDs. Furthermore, I found that LsAtg8 lipidation and mitochondrial degradation are highly suppressed by overexpression of LsAtg4. Surprisingly, bulk autophagy was also strongly suppressed in nitrogen-starved *L. starkeyi* cells undergoing giant LD formation. Finally, impaired LsAtg8 lipidation in LsAtg4-overexpressing *L. starkeyi* cells caused an alteration in LD expansion. These results raise the possibility that a potential autophagy-unrelated function of lipid-conjugated LsAtg8 could be linked to giant LD formation.

Taken together, the findings presented in this thesis reveal that mitochondrial dynamics and autophagy are tightly regulated in positive and negative ways, respectively, during LD expansion in *L. starkeyi* cells.

Chapter 2. Mitochondrial dynamics and autophagy during giant lipid droplet formation in oleaginous yeast

2-1 INTRODUCTION

Lipid droplets (LDs), known as fat reservoirs, are evolutionarily conserved organelles. LDs have been reported to be ubiquitous and dynamic, composed of a single neutral lipid core (mainly triacylglycerols (TAGs) and sterol esters) covered by a phospholipid monolayer and proteins. (Wilfling et al., 2014). Accumulating evidence suggests that LDs utilize mechanisms to move within the cells and make multiple contacts with various organelles, such as the ER, peroxisomes, lysosomes, Golgi, and mitochondria [6,7]. Through their functions from biogenesis to breakdown, such as lipid synthesis, lipid hydrolysis, and lipid distribution, LDs play critical roles in not only energy buffering but also stress alleviation, lipotoxicity prevention, organelle homeostasis, membrane homeostasis, and autophagosome biogenesis [2-5]. Although it seems likely that LDs act in a wide range of cellular activities, the simultaneity of those activities makes it difficult to study their mechanisms, leaving us at the very beginning stage of understanding.

Recent studies have highlighted that a portion of mitochondria, named PDM (peridroplet mitochondria), attaches to LDs in mammals, such as rat skeletal muscle [75], mouse heart muscle [73], mouse brown adipose tissue (BAT) [76], and hepatocytes [86]. Mitochondria, besides their functions in ATP and heat generation, are also critically involved in lipid synthesis (lipogenesis and TAG synthesis) and lipid consumption (beta-oxidation) [77-79]. Mitochondria-LD interactions increase upon starvation conditions, raising the possibility that those interactions promote fatty acid oxidation in mitochondria [82-83]. However, on the other hand, PDM may have a higher capacity to oxidize pyruvate and malate for TAG synthesis but a low capacity for fat oxidation, compared to cytosolic mitochondria (CM), which enabled the expansion of LDs [85]. Furthermore, mitochondria can actually undergo both lipid synthesis and oxidation at the same time in BAT and immune cells[87-89], which challenges the conventional concept that mitochondria cannot support those processes simultaneously [90, 91]. However, since PDM have been reported to have bioenergetics, proteome, cristae organization, and dynamics distinct from CM [92], their function in LD formation remains largely unexplored.

Mitochondrial degradation by autophagy, termed mitophagy, is thought to be critical for cellular fat homeostasis [101, 106]. Mitophagy is a highly conserved process that selectively wraps mitochondria with autophagosomes (or mitophagosomes in mitophagy) and delivers them to lysosomes (vacuoles in yeast) for their degradation [100, 116]. Recent studies have reported that mitophagy is significantly activated in BAT after chronic cold exposure [107] and it also functions in the alleviation of high-fat diet-induced obesity and diabetic

cardiomyopathy [108, 109]. Besides mitochondrial degradation, mitochondrial dynamics is involved in LD homeostasis. In murine brown adipose tissue, a defect in mitochondrial fusion by deficiency of Mfn2, a GTPase that controls mitochondrial outer membrane fusion [111], impairs mitochondria by reducing β-oxidation and mitochondrial respiration while it promotes LD accumulation and FA efflux from cells [84]. How mitochondrial dynamics and degradation affect or are affected by LD is still unclear.

For further understanding of the crosslink between mitochondria and LDs, the oleaginous yeast *Lipomyces starkeyi* serves as a unique model. Among unicellular eukaryotes, *L. starkeyi* is one of the most attractive organisms that can metabolize a wide variety of carbon and nitrogen sources and accumulate giant LDs above 65% of its dry weight [112], being a striking candidate for industrial oil production. Lipid accumulation in *L. starkeyi* can be affected by various factors such as the carbon-to-nitrogen ratio, pH, temperature, aeration speed, inoculum age, fermentation time, and inhibitors [40, 113], which result in uncertainty to the final lipid yield. A recent study has reported that wild-type *L. starkeyi* NBRC10381 cells can accumulate lipid content up to 85% of their dry weight under nitrogen-limited culture conditions [114].

In this study, despite the difficulties in genetic manipulations of this yeast, I succeeded to visualize mitochondria in *L. starkeyi* NRRL Y-1388 using mito-DHFR-mCherry, a mitochondrial matrix-targeted red fluorescent marker fused with dihydrofolate reductase, making it a potential yeast model for studying mitochondria and LDs [115]. Next, I investigated mitochondrial shape and degradation during LD formation-inducing conditions using *L. starkeyi*. I found that under nitrogen-starvation conditions, mitochondria form tubular and sheet-like shapes in close proximity to a giant LD. Notably, mitochondrial degradation was hardly seen in those nitrogen-starved cells which was likely to be caused by suppression of autophagy. By contrast, carbon-starved *L. starkeyi* cells underwent degradation of mitochondria without giant LD formation. Overexpression of LsAtg4, a sole protease that regulates autophagy through processing and delipidation of Atg8 [117], can block LsAtg8 lipidation, thereby suppressing autophagy and mitochondrial degradation in carbon-starved *L. starkeyi* cells. These observations raise the possibility that LD expansion is promoted in nitrogen-depleted *L. starkeyi* cells in a manner independent of mitochondrial degradation and autophagy.

2-2 RESULTS

2-2-1 *L. starkeyi* cells expressing a mitochondrial matrix-targeted fluorescent probe grow at near wild-type levels

The mitochondrial matrix-targeted mito-DHFR-mCherry fusion protein is an established tool to investigate mitochondrial shaping and mitophagy in *S. cerevisiae* [118]. To apply this approach to *L. starkeyi*, I cloned a mito-DHFR-mCherry expression cassette containing *L. starkeyi TEF1* 5'-flanking promoter (P_{LsTEF1}) and 3'-flanking terminator (T_{LsTEF1}) regions into pKS-18S-hph [119], a vector that has been designed to efficiently integrate a gene of interest into the *L. starkeyi* chromosomal 18S rDNA locus under hygromycin selection (Figure 2-1A). I performed transformation using the 18S-mito-DHFR-mCherry-hph cassette and generated hygromycin-resistant *L. starkeyi* cells expressing mito-DHFR-mCherry from the 18S rDNA locus.

To verify whether mito-DHFR-mCherry is targeted to mitochondria in the *L. starkeyi* transformants, I performed fluorescence microscopy for cells stained with MitoBright LT Green, a mitochondria-specific vital dye. When grown under fermentable conditions, both *S. cerevisiae* and *L. starkeyi* cells exhibited mCherry signals mostly overlapped with MitoBright LT Green signals, indicating that mito-DHFR-mCherry primarily localizes to mitochondria (Figure 2-1B). I further confirmed that *L. starkeyi* cells expressing mito-DHFR-mCherry grow normally like the wild-type cells at 26°C and 30°C on a YP medium containing dextrose, galactose, or glycerol, whereas they all do not grow at 37°C, a non-permissive temperature for *L. starkeyi* wild-type cells (Figure 2-1C). Thus, it seems promising that mito-DHFR-mCherry can serve as a mitochondria-specific probe without significantly affecting cellular fitness in *L. starkeyi*.

2-2-2 Mitochondria form elongated tubular structures in *L. starkeyi* cells under prolonged nitrogen starvation

Lipid synthesis and accumulation can generally be induced or suppressed by nitrogen or carbon deprivation, respectively [40]. To investigate mitochondrial morphology during LD expansion in *L. starkeyi*, cells expressing mito-DHFR-mCherry, which is a mitochondrial matrix-targeted probe consisting of dihydrofolate reductase (DHFR) and mCherry [115], were grown in nutrient-complete medium (SDCA) to $OD_{600} \approx 1$, transferred to nitrogen-depleted medium (SD-N: -N) or carbon-depleted medium (SN-D: -C) to induce or suppress giant LD formation, respectively. I performed fluorescence microscopy to quantify LD size using

BODIPY 493/503 staining and observed mitochondrial morphology with mito-DHFR-mCherry (22-2). As expected, LD expansion was highly induced under nitrogen starvation (Figure 2-2A and C), whereas it was strongly suppressed under carbon starvation (Figure 2-2B and C). In addition, I found that mitochondria formed elongated tubular structures that seemed to be in close proximity to a single giant LD in nitrogen-depleted cells (Figure 2-2A). By contrast, most of the mitochondria kept fragmented and distributed at the cell periphery in carbon-depleted cells (Figure 2-2B).

2-2-3 Prolonged nitrogen starvation leads to mitochondrial elongation and mitochondria-LD proximity.

To examine mitochondrial morphology and distribution in greater detail, *L. starkeyi* cells grown in media lacking nitrogen (-N) for 24 h and 72 h were observed using scanning electron microscopy (SEM) (Figure 2-3A). I found that the number of mitochondria drastically decreased, whereas the size of each mitochondrion only slightly increased in nitrogen-depleted cells at the 72 h time point, compared with those at the 24 h time point (Figure 2-3B and C).

To quantitatively analyze the mitochondrial shape, I first categorized all the mitochondria into small-sized (mito-S) and large-sized (mito-L) groups, using the average size of each mitochondrion ($\approx$ 0.08 μm^2) as a threshold. I found that mito-L exhibit high variability in shape (Figure 2-3D), and that there is no significant difference in the mito-S/L ratios of cells between the 24 h and 72 h time points (Figure 2-3E). Next, I investigated the shape of mitochondria by their length and aspect ratio, which led us to estimate mitochondrial elongation. Our data indicated that compared with those at the 24 h time point, both mito-S and -L become longer and more elongated at the 72 h time point (Figure 2-3F and G).

I also examined two-dimensional SEM images to quantify the mitochondria-LD proximity in cells under nitrogen starvation. I found that the percentage of cells containing mitochondria in close proximity to LD at the 72 h time point was significantly higher than that at the 24 h time point (Figure 2-3H). Moreover, the average length of the mitochondria-LD proximity sites at the 72 h time point was longer than that at the 24 h time point (Figure 2-3I). These data are consistent with the idea that the mitochondria-LD proximity increase during LD expansion in *L. starkeyi* cells under prolonged nitrogen starvation.

2-2-4 Mitochondria form elongated tubules and sheet-like structures in close proximity to a giant LD

To clarify the shape of mitochondria in close proximity to LDs, I performed array tomography, one of the techniques to reveal 3D ultrastructure termed volume electron microscopy (vEM). Cells were subjected to chemical fixation, embedded in a resin, cut into an array of ultrathin sections, imaged with SEM (Figure 2-4A and B), and reconstituted into a 3D data set (Figure 2-4C and 2-5). In nitrogen-depleted cells at the 24 h time point, most mitochondria were rod-like in shape, whereas a small fraction of mitochondria exhibited tubular morphologies (Figures 2-4C and 2-5). In those cells, only a few mitochondria were in close proximity to LDs (Figures 2-4C, 2-5, and 2-6). In nitrogen-depleted cells at the 72 h time point, most mitochondria, which became smaller in number and bigger in volume compared to those at the 24 h time point (Figure 2-6), were elongated tubules or sheet-like structures (Figures 2-4C and 2-5). Notably, many of them were in close proximity to a giant LD (Figures 2-4C, 2-5, and 2-6). Those observations raise the possibility that mitochondria remodel their shape concurrently with LD expansion and augment their LD-proximity in nitrogen-depleted *L. starkeyi* cells.

2-2-5 Mitochondrial degradation and autophagy are strongly suppressed in nitrogen-depleted *L. starkeyi* cells

To investigate degradation of mitochondria in *L. starkeyi* cells with or without LD expansion, I performed mito-DHFR-mCherry processing assays for cells under nitrogen (-N) and carbon (-C) starvation (Figure 2-7A and B). Upon mitochondrial degradation, this mitochondrial matrix-localized probe is transported to the vacuole and processed to generate free mCherry. As mCherry is quite resistant to vacuolar proteases, its accumulation semi-quantitatively indicates mitochondrial degradation flux. Surprisingly, I found that mitochondrial degradation was highly induced by carbon depletion, whereas it was strongly suppressed by nitrogen depletion. These results imply that *L. starkeyi* is a unique organism, as mitochondrial degradation is induced under nitrogen starvation in most eukaryotes including the baker's yeast *S. cerevisiae* and mammals [101, 122, 123].

Next, to analyze the autophagy levels in *L. starkeyi* cells, I constructed an autophagy assay strain expressing mCherry-LsAtg8. Atg8 is an evolutionarily conserved ubiquitin-like protein acting in autophagosome formation [124]. Upon autophagy induction in *S. cerevisiae* cells, Atg8 is upregulated and its C-terminal arginine 117 is cleaved by Atg4, a cysteine protease essential for autophagy, to expose glycine 116 for its conjugation to the phospholipid phosphatidylethanolamine (PE) [117, 125]. Atg8-PE localizes on the surface and lumen of autophagosomes, and Atg8-PE on the autophagosomal surface is cleaved by Atg4 to generate

free Atg8. When N-terminally tagged with mCherry, the autophagosomal lumen-localized mCherry-Atg8 is transported to the vacuole and processed to generate free mCherry. Thus, mCherry-Atg8 processing assay is a useful tool to monitor the autophagy flux [126].

Surprisingly, even though it was expressed under a strong constitutive promoter, the mCherry-Atg8 levels significantly decreased in nitrogen-depleted *L. starkeyi* cells (Figure 2-7C). Under the same conditions, free mCherry was hardly accumulated, indicating that autophagy was merely induced (Figure 2-7D). By contrast, both mCherry-Atg8 and free mCherry levels were highly increased in carbon-depleted *L. starkeyi* cells (Figure 2-7C and D). These results support the notion that LD forms a giant sphere independently of autophagy.

2-2-6 Mitochondrial degradation is strongly reduced by autophagy suppression in carbon-depleted *L. starkeyi* cells

To ask if mitochondrial degradation under carbon starvation is mediated via autophagy, I developed a method to suppress autophagy by overexpression of LsAtg4 in *L. starkeyi* cells. First, I constructed an *S. cerevisiae* mitophagy assay strain (with mito-DHFR-mCherry) overexpressing Atg4, by replacing the endogenous *ATG4* promoter with the strong constitutive GPD promoter. To examine mitophagy, wild-type, Atg4-overexpressing (*GPD-ATG4*), and atg32-null (defective in mitophagy) cells were grown under carbon starvation (-C) and subjected to western blotting for generation of free mCherry (Figure 2-8A and B). Overexpression of Atg4 caused a strong suppression in mitophagy under carbon starvation, probably due to a reduction in the Atg8-PE levels (Figure 2-8A).

Next, I asked whether bulk autophagy can also be suppressed by overexpression of Atg4. To this end, western blot analysis was performed for *S. cerevisiae* cells expressing Tdh3-mCherry, a cytoplasmic marker that is transported to vacuoles in an Atg7-dependent manner and processed to generate free mCherry. Wild-type, *GPD-ATG4*, and atg7-null (defective in autophagy) cells expressing Tdh3-mCherry were grown under carbon starvation (-C) and subjected to western blotting for generation of free mCherry. Similarly to mitophagy, bulk autophagy was significantly suppressed, and the Atg8-PE levels were reduced in cells overexpressing Atg4 (Figure 2-8C and D). These data suggest that in *S. cerevisiae* cells, overexpression of Atg4 leads to a decrease in Atg8-PE, thereby suppressing autophagosome formation for mitophagy and bulk autophagy.

Based on the above data on *S. cerevisiae* cells, I generated *L. starkeyi* strain overexpressing LsAtg4-3V5 and attempted to suppress autophagy. Wild-type and LsAtg4-overexpressing *L. starkeyi* cells with mito-DHFR-mCherry were grown under carbon starvation (-C) and

subjected to western blotting for generation of free mCherry to quantify mitochondrial degradation (Figure 2-9A and B). I found that mitochondrial degradation was strongly suppressed in cells overexpressing LsAtg4. Under the same conditions, the Atg8-PE levels were decreased, whereas the free Atg8 levels were increased (Figure 2-9A). These results are consistent with the idea that mitochondrial degradation in carbon-depleted *L. starkeyi* cells is a bona fide mitophagy.

I also noticed that despite of strong suppression in mitophagy and autophagy, which were similarly seen in nitrogen-depleted *L. starkeyi* cells undergoing giant LD formation, *L. starkeyi* cells overexpressing LsAtg4 exhibited neither LD expansion nor significant alteration in mitochondrial shape under carbon starvation (Figure 2-10A-E). Thus, it seems unlikely that suppression of mitophagy and autophagy is sufficient to promote giant LD formation and mitochondrial remodeling in carbon-depleted *L. starkeyi* cells.

2-2-7 LD expansion is partially suppressed by overexpression of LsAtg4 in *L. starkeyi* cells under nitrogen starvation

To investigate how overexpression of LsAtg4 affects giant LD formation, I performed BODIPY staining for LsAtg4 overexpressing *L. starkeyi* cells grown in -N media (Figure 2-11). I found that under nitrogen starvation, which highly induces giant LD formation, the number of LDs was increased in LsAtg4 overexpressing *L starkeyi* cells, whereas the amount of LDs had no significant change (Figure 2-12). Especially at the 24 h time point, 77.1% of *LsATG4* overexpressing cells contained multiple small LDs, whereas only 19.1% of wild-type cells contained multiple small LDs (Figure 2-11B). Given the observations that mitochondrial degradation and LsAtg8 lipidation are only slightly induced even in nitrogen-starved *L starkeyi* wild-type cells (Figure 2-7), I speculate that the increased LD number is not caused by autophagy suppression in LsAtg4 overexpressing *L starkeyi* cells. To test this idea, I did the same analysis in -C media. I found that both LD number and amount are not affected by *LsATG4* overexpression in carbon-depleted cells. These results raise the possibility that LD expansion might not affected by autophagy suppression, but by increased LsAtg8-PE levels or some unknown mechanisms in LsAtg4 overexpressing *L starkeyi* cells.

2-3 DISCUSSION

The interaction between mitochondria and lipid droplets in energy metabolism has been well studied in metabolomics. However, the relationship between these organelles in their physical dynamics and morphology changes remains poorly explored.

In this study, I successfully introduced the mitochondrial marker mito-DHFR-mCherry into an oleaginous yeast *L. starkeyi*, establishing a tool to analyze mitochondrial shape and degradation in cells undergoing prominent lipid droplet formation (Figure 2-1). Using an *L. starkeyi* strain expressing mito-DHFR-mCherry, I successfully made the first-time observation of mitochondria behaviors in oleaginous yeast cells (Figure 2-2). I found that mitochondria kept fragmented in cells without giant LD formation under carbon starvation. In contrast, mitochondria were markedly tubulated in close proximity to a giant LD in cells under nitrogen starvation.

To have a more comprehensive understanding, I also analyzed mitochondrial morphology and mitochondria-LD proximity using SEM (Figures 2-3, 2-4, 2-5, 2-6). The quantitative 2D-SEM and array tomography-based 3D-vEM revealed that mitochondria became elongated to form tubules and sheets that were in close proximity to a giant LD under prolonged nitrogen starvation (Figures 2-3, 2-4, 2-5). Moreover, the frequency of mitochondria-LD proximity increased during LD expansion. However, given the fact that a giant LD occupies most of the intracellular space after 72 h of nitrogen deprivation, we do not exclude the possibility that the high mitochondria-LD proximity is due to space limitations. Furthermore, studies in mammalian cells have shown that mitochondrial fusion plays a crucial role in mitochondria-LD fatty acid trafficking and mitochondrial-LD association [77, 84, 127]. Therefore, it would be interesting to investigate whether mitochondrial tubules and sheets are formed by increased mitochondrial fusion and/or reduced mitochondrial fission in *L. starkeyi*. Thus, elucidating how mitochondrial fusion and fission events affect the mitochondria-LD proximity in *L. starkeyi*, and how the mitochondrial proximity contributes to giant LD formation in *L. starkeyi* await further investigations.

My study also reveals a unique aspect of *L. starkeyi* in its response to nitrogen starvation (Figure 2-7). Unlike other eukaryotic organisms whose nutrient depletion (nitrogen, carbon, amino acids, etc.) is a common method to induce autophagy-related events [101, 128], *L. starkeyi* exhibited only a minimal level of autophagy and mitochondrial degradation under nitrogen starvation (Figure 2-7), whereas it underwent those catabolic events at a relatively high levels under carbon starvation. These observations raise intriguing questions about the relation between autophagic catabolism and giant LD formation. Currently, increasing

evidence supports the idea that there is a specific interplay between autophagy and LD formation and degradation, though the detailed mechanisms remain obscure. In hepatocytes and the model of obesity, autophagy inhibition by pharmaceuticals or disrurption of autophagy regulators contributes to TAG synthesis and LD accumulation. Conversely, excess lipid contents suppress the expression of autophagy regulators [62, 63]. Furthermore, in *S. cerevisiae*, complete disruption of LD biogenesis and TAG synthesis results in suppression of starvation-induced autophagy [129-131]. These findings raise the question of whether autophagy is only maintained when the level of lipid droplet formation remains within a moderate range. Further studies are necessary to clarify if loss of LD expansion induces mitophagy and autophagy in nitrogen-depleted *L. starkeyi* cells.

My finding that mitochondrial degradation under carbon starvation is strongly reduced by autophagic suppression via overexpression of LsAtg4 is consistent with the idea that this catabolic event is bona fide mitophagy (Figure 2-9A and B). Currently, the molecular mechanisms and physiological functions of mitophagy in *L. starkeyi* remain largely unknown. I have performed a BLAST search and found that *L. starkeyi* does not seem to have an obvious Atg32 homolog. Although gene knock-in/-out and expression using a plasmid system are technically quite difficult in *L. starkeyi*, future attempts are needed to identify and characterize protein(s) essential for mitophagy and to prove that mitophagy and autophagy are dispensable for giant LD formation in *L. starkeyi* cells.

In addition, LD split caused by *LsATG4* overexpression under nitrogen-depletion conditions, where autophagy is barely induced (Figure 2-10), also implies that *LsATG4* overexpression may have a special function on LD expansion in *L. starkeyi*. Although the molecular mechanism is not fully understood, I speculate that LsAtg8 could be involved in LD expansion. In hepatocytes and cardiac myocytes, LC3 (the mammalian homolog of Atg8) along with its lipidation system was found to be required for LD accumulation [67, 68]. In yeast, Atg8 is found to function in maintaining LD quantity but not LD accumulation, and it is independent of its lipidation system [69]. Based on these findings, I hypothesize that overexpression of LsAtg4 may affect LD dynamics by altering Atg8 lipidation in *L. starkeyi*. Nevertheless, I still cannot rule out the possibility that overexpression of LsAtg4 may influence LD dynamics in a direct or indirect manner, independent of LsAtg8 lipidation system. Further research is required to verify the function of LsAtg4 and LsAtg8 in LD dynamics.

Oils derived from oleaginous microorganisms represent a compelling substitute for oils extracted from plants and animals due to their independence from environmental factors such as space and climate and their high lipid production efficiency without posing competition with

food resources [132]. Within all those oleaginous microorganisms, the oleaginous yeast *L. starkeyi* emerges as a notable candidate for single-cell oil and oleochemical production as its outstanding storage lipids production ability [112, 114]. Our findings on the regulation of mitochondria-associated LD formation in *L. starkeyi*, may provide valuable guidance into the bioengineering of *L. starkeyi* to increase the yield of biofuels.

2-4 MATERIALS AND METHODOLOGIES

2-4-1 Yeast strains and growth conditions

Yeast strains and plasmids used in this study are described in Tables 1 and 2. Standard genetic and molecular biology methods were used for *Saccharomyces cerevisiae* strains. *L. starkeyi* NRRL Y-1388 (distributed from RIKEN BioResource Research Center, Japan) and *S. cerevisiae* BY4741 cells were incubated at 26ºC and 30ºC, respectively, in YPD medium (1% yeast extract, 2% peptone, and 2% dextrose) or complete medium SDCA (0.17% yeast nitrogen base without amino acids and ammonium sulfate, 0.5% ammonium sulfate with 0.5% casamino acids containing 2% dextrose) supplemented with necessary amino acids and nucleotide bases. For nitrogen depletion, cells were pregrown to mid-log phase in SDCA and transferred to SD-N medium (0.17% yeast nitrogen base without amino acids and ammonium sulfate plus 2% dextrose). For carbon depletion, cells were pregrown to mid-log phase in SDCA and transferred to SN-D medium (0.17% yeast nitrogen base without amino acids and ammonium sulfate and ammonium sulfate, 0.5% ammonium sulfate with 0.5% casamino acids).

2-4-2 Growth assay

L.starkeyi wild-type and mito-DHFR-mCherry-expressing cells pregrown in YPD medium were harvested by centrifugation, resuspended in water corresponding to $OD_{600} \approx 1$, and aliquoted to 1:5, 1:25, and 1:125 dilutions. The cell suspensions were then spotted onto YPD (1% yeast extract, 2% peptone, and 2% dextrose), YPGal (1% yeast extract, 2% peptone, and 2% galactose), and YPGly (1% yeast extract, 2% peptone, and 3% glycerol) plates containing 2% agar, and incubated at 26°C, 30°C, and 37°C for 2 days.

2-4-3 Construction of the DNA cassettes encoding mito-DHFR-mCherry, *LsATG4-3V5*, and *mCherry-LsATG8* for *L. starkeyi*

The gene overexpression strategy for *L. starkeyi* is based on the method as developed previously [119]. The construction of pKS-18S-mito-DHFR-mCherry-hph, encoding the *Ls18S rDNA* (0.5 kbp), *LsTDH3* promoter (1.0 kbp), *LsTEF1* promoter (1.2 kbp) (P_{LsTEF1}), mito-DHFR-mCherry (1.5 kbp), *LsTEF1* terminator (0.5 kbp) (T_{LsTEF1}), hygromycin B phosphotransferase from *Escherichia coli* (1.0 kbp) (hph), *LsTDH3* terminator (0.5 kbp) (TLsTDH3), and *Ls18S rDNA* (0.8 kbp), is described in our previous study [115].

For overexpression of LsAtg4 in mito-DHFR-mCherry expressing cells, I first substituted hph of pKS-18S-mito-DHFR-mCherry-hph with nat encoding nourseothricin N-acetyltransferase from *Streptomyces noursei* (0.6 kbp). The resulting plasmid was named as pKS-18S-mito-DHFR-mCherry-nat. The fragment of *LsATG4(cDNA)-3V5* (1.6 kbp) was amplified by PCR using pEX-A2J2-LsATG4-3V5, a custom-made plasmid from Eurofinsgenomics, as a template, 5'-tgctaacagcttacttctacagGGAATGGACAATATTCAACGTTTTGTGAACT-3' and 5'-CTAagcaccGGTGGAGTCTAG-3' as primers. The vector pKS-18S-nat encoding *Ls18S rDNA* (0.5 kbp), *LsTDH3* promoter (1.0 kbp), Ls*TEF1* promoter (1.2 kbp) (P_{LsTEF1}), *LsTEF1* terminator (0.5 kbp) (T_{LsTEF1}), nat (0.6 kbp) (nat), *LsTDH3* terminator (0.5 kbp) (T_{LsTDH3}), and *Ls18S rDNA* (0.8 kbp) was amplified by PCR using pKS-18S-mito-DHFR-mCherry-nat as a template, and 5'-CTAGACTCCACCggtgctTAGaaggttttcgtgctcttgtttg-3' and 5'-ctgtagaagtaagctgttagca-3' as primers. These PCR-amplified fragment and vector were seamlessly fused to create circular plasmid DNA using an In-Fusion HD Cloning Kit (Takara Bio). The resulting plasmid was named as pKS-18S-LsATG4-3V5-nat. The final DNA cassette was amplified by PCR using pKS-18S-LsATG4-3V5-nat as a template and the primers 5'-GCTTCTTCGGAAGCTCTTTG-3' and 5'-CGACTATATCTTAAGCCGCA-3'.

For overexpression of mCherry-LsAtg8 in wild-type *L. starkeyi* cells, the fragment of mCherry (0.1 kbp) was amplified by PCR using pKS-18S-mito-DHFR-mCherry-hph as a template, and 5'- tgctaacagcttacttctacagGGAGTGAGCAAGGGCGAGGAGGATA-3', and 5'-CTTGTACAGCTCGTCCATGC-3' as primers. The fragment of *LsATG8 (cDNA)* (357 bp) was amplified by PCR using pEX-A2J2-LsATG8, a custom-made plasmid from Eurofinsgenomics,as a template and 5'-GCATGGACGAGCTGTACAAGATGCGTTCTAAGTTCAAAGACG-3'and 5'-CTATTGAGCTCCAAATGTGTTC-3' as primers. These two fragments and the pKS-18S-nat fragment, which was amplified by PCR using pKS-18S-mito-DHFR-mCherry-nat as a template, and 5'-GAACACATTTGGAGCTCAATAGaaggttttcgtgctcttgtttg-3' and 5'-ctgtagaagtaagctgttagca-3' as primers, were seamlessly fused to create circular plasmid DNA using an In-Fusion HD Cloning Kit (Takara Bio). The resulting plasmid was named as pKS-18S-mCherry-LsATG8-nat. The final DNA cassette was amplified by PCR using pKS-18S-mCherry-LsATG8-nat as a template and 5'-GCTTCTTCGGAAGCTCTTTG-3' and 5'-CGACTATATCTTAAGCCGCA-3' as primers.

2-4-4 Transformation for *L. starkeyi* strains

Transformation for *L. starkeyi* was performed as reported previously [133]. Cells were pregrown in 7 ml of YPD for 2–3 days to the stationary phase ($OD_{600} \approx 10$), diluted in 30 ml of YPD, and grown at 26ºC overnight. Cells at $OD_{600} = 10$ were harvested, washed once with 10 ml of water, and resuspended in 1 ml of 100 mM LiAc. After transferred to a 1.5 ml tube, the cell suspension was subjected to centrifugation, resulting in cell pellets of 50 µl. Cells were mixed with 1 µg DNA cassette, 15 µl of ssDNA (2 mg/ml), 30 µl of 1 M LiAc, and 240 µl of 50% PEG, resuspended thoroughly with vortexing and pipetting, and incubated at room temperature for 4 h. After treated with a heat shock at 40ºC for 5 min, cells were harvested by centrifugation, resuspended in 1 ml of YPD, and incubated at room temperature. Cells were spread on a YPD plate (1% yeast extract, 2% peptone, 2% dextrose, 2% agar) containing 100 mg/ml hygromycin or 20 mg/ml nourseothricin for selecting transformants and incubated at 26ºC for 7–10 days.

2-4-5 Fluorescence microscopy

L. starkeyi cells were observed using a Pulse-SIM BZ-X800 microscope (Keyence) equipped with a 100 × objective lens (CFI Apochromat TIRF 100XC Oil, NA: 1.49; Nikon), filter sets for GFP and mCherry (BZ-X filter GFP and BZ-X filter TRITC, respectively; Keyence) and an optical sectioning module (BZ-H4XF; Keyence).

2-4-6 Preparation of specimen for electron microscopy

L. starkeyi cells were pregrown in SDCA to $OD_{600} \approx 1$, transferred into SD-N and SN-D media, and incubated at 26ºC for another 24 h and 72 h. Previously developed $KMnO_4$ fixation method [134] was adjusted and utilized for the specimen preparation. Cells in the medium were fixed by adding an equal volume of fixative (5% glutaraldehyde in 0.1 M PB buffer). Cells are then collected by gentle filtration through a filter (Nano Percolator, JEOL, Tokyo) and immediately mixed and embedded in 2% agarose. The cell blocks were cut into small cube and washed twice with 0.1 M PB buffer (pH 7.4) and postfixed with 1.5% KMnO4 for 20 h. The specimens were washed three times with water and pre-stained with a 1.5% aqueous solution of uranyl acetate for 1.5 h. The dehydration was performed using Acetone in the following series: 30% Acetone 10 min, 50% Acetone 10 min, 70% Acetone 10 min, 80% Acetone 10 min, 90 % Acetone 10 min, 95% Acetone 10 min, and 100% Acetone 30 min for twice. Subsequently, dehydrated specimens were infiltrated and embedded into Spurr resin (Polyscience, PA) in the following series: Acetone: Resin = 3:1, 4 h; Acetone: Resin = 1:1,

overnight; Acetone: Resin = 3:1, 4 h; 100 % Resin, overnight and polymerized in 65ºC for 48 h. The specimens were observed using a field emission scanning electron microscope (FE-SEM) (JSM-IT800; JEOL, Tokyo). The images were acquired using software (SEM Supporter; System in Frontier, Tokyo) and a backscattered electron detector. The conditions of SEM observation were set as follows: working distance = 8.0 mm, pixel size = 5.56 nm/pixel, image size = 7680 × 5760 pixels.

For tomography, resin-embedded cell blocks were trimmed into 500 nm x 500 nm for serial sections with a 50 nm thickness using an ultramicrotome (Leica ultramicrotome ARTOS 3D) with a diamond knife (UltraJumbo 35, Diatome). The serial sections were cut into ribbons, placed on a silicon wafer, and stained with an aqueous solution of 1% uranyl acetate for 10 min, followed by 10 min with lead citrate.

2-4-7 Array tomography

The specimens were observed using a field emission scanning electron microscope (FE-SEM) (JSM-IT800; JEOL, Tokyo). Serial section images were acquired using software (SEM Supporter; System in Frontier, Tokyo) as a backscattered electron image. The conditions of SEM observation were set as follows: acceleration voltage =5KeV, working distance = 8.0 mm, pixel size = 5.56 nm/pixel, image size = 7680 × 5760 pixels.Data processing for three-dimensional reconstruction

Serial images were aligned using SIFT (Fiji plugin “Linear Stack Alignment with SIFT”) and Microscopy Image Browser 2.70 (https://mib.helsinki.fi/index.html). Segmentation and deep learning of mitochondrial shape were performed using Napari-Philow (an interactive deep learning-based platform for 3D datasets, https://www.napari-hub.org/plugins/napari-PHILOW). 3D reconstruction of mitochondria was performed using Amira 3D 2022.2 (ThermoFisher Scientific).

2-4-8 Western blotting

Protein samples corresponding to 0.1 OD_{600} units of *S. cerevisiae* and *L. starkeyi* cells were separated by SDS-PAGE, transferred to a PVDF membrane by western blotting, and subjected to immunodecoration with primary antibodies raised against mCherry (1:2,000, Abcam ab125096) and Atg8 (1:2,000, a kind gift from Hitoshi Nakatogawa, Tokyo Institute of Technology, Japan). Samples corresponding to 0.02 OD_{600} units of *S. cerevisiae* and *L. starkeyi* cells were analyzed using anti-beta actin (1:20,000, Abcam ab8224) as a loading control. After

treatment with the secondary antibodies, horseradish peroxidase (HRP)-conjugated rabbit anti-mouse IgG (H + L)
for anti-mCherry and anti-beta actin, and goat anti-rabbit IgG (H + L) for anti-Atg8 followed by the enhanced chemiluminescence reagent Western Lightning Plus-ECL (NEL103001EA, PerkinElmer), proteins were detected using a luminescent image analyzer (FUSION Solo S; Vilber). Quantification of the signals was performed using FUSION Solo S (Vilber).

2-4-9 Lipid droplet assay

L. starkeyi cells pregrown in SDCA medium were transferred to SD-N and SN-D media, cultured at 26ºC, collected at the 24 h, 48 h, and 72 h time points, and observed under a fluorescence microscope. All experiments were repeated three times independently. More than 40 cells were selected randomly from microscopic images for different culture conditions at each time point. The number of cells (N) and the area of LD-specific BODIPY signals (a) was measured by ImageJ (National Institutes of Health, USA). The average area of LDs in each cell (A) was calculated by A = a/N.

3 REFERENCES

1. **Wilfling, F., Haas, J. T., Walther, T. C. and Farese, R. V., Jr** (2014). Lipid droplet biogenesis. *Curr Opin Cell Biol*., **29**, 39–45.

2. **Welte, M. A. and Gould, A. P.** (2017). Lipid droplet functions beyond energy storage. *Biochimica et biophysica acta.* Molecular and cell biology of lipids, **1862**(10 Pt B), 1260–1272.

3. **Petan, T., Jarc, E., & Jusović, M.** (2018). Lipid Droplets in Cancer: Guardians of Fat in a Stressful World. *Molecules*., **23**(8), 1941.

4. **Olzmann JA, Carvalho P.** (2019) Dynamics and functions of lipid droplets. *Nat Rev Mol Cell Biol.*, 2019., **20**(3), 137–155.

5. **Shatz, O., Holland, P., Elazar, Z. and Simonsen, A.** (2016). Complex Relations Between Phospholipids, Autophagy, and Neutral Lipids. *Trends Biochem Sci*., **41**(11), 907–923.

6. **Valm, A. M., Cohen, S., Legant, W. R., Melunis, J., Hershberg, U., Wait, E., Cohen, A. R., Davidson, M. W., Betzig, E. and Lippincott-Schwartz, J.** (2017). Applying systems-level spectral imaging and analysis to reveal the organelle interactome. *Nature*, **546**(7656), 162–167.

7. **Cohen, S., Valm, A. M., and Lippincott-Schwartz, J.** (2018). Interacting organelles. *Curr Opin Cell Biol.*, **53**, 84–91.

8. **Yang, Z. and Klionsky, D. J.** (2010). Mammalian autophagy: core molecular machinery and signaling regulation. *Curr Opin Cell Biol*. , **22**(2), 124–131.

9. **Mijaljica, D., Prescott, M. and Devenish, R. J.** (2011). Microautophagy in mammalian cells: revisiting a 40-year-old conundrum. *Autophagy*, **7**(7), 673–682.

10. **Massey, A., Kiffin, R. and Cuervo, A. M.** (2004). Pathophysiology of chaperone-mediated autophagy. *Int J Biochem Cell Biol*. , **36**(12), 2420–2434.

11. **Yorimitsu, T. and Klionsky, D. J.** (2005). Autophagy: molecular machinery for self-eating. *Cell Death Differ*., 12 Suppl 2(Suppl 2), 1542–1552.

12. **Chun, Y. and Kim, J.** (2018). Autophagy: An Essential Degradation Program for Cellular Homeostasis and Life. *Cells*, **7**(12), 278.

13. **Liu, H., Yuan, M., Mitra, R., Zhou, X., Long, M., Lei, W., Zhou, S., Huang, Y. E., Hou, F., Eischen, C. M. and Jiang, W.** (2022). CTpathway: a CrossTalk-based pathway enrichment analysis Mo Peemethod for cancer research. *Genome Med*., **14**(1), 118.

14. **Okamoto K.** (2014). Organellophagy: eliminating cellular building blocks via selective autophagy. *J Cell Biol*., 205(4), 435–445.

15. Reggiori, F. and Molinari, M. (2022). ER-phagy: mechanisms, regulation, and diseases connected to the lysosomal clearance of the endoplasmic reticulum. *Physiol Rev.*, 102(3), 1393–1448.

16. **Papandreou, M. E. and Tavernarakis, N.** (2019). Nucleophagy: from homeostasis to disease. *Cell Death Differ*. , **26**(4), 630–639.

17. **Shin D. W.** (2020). Lipophagy: Molecular Mechanisms and Implications in Metabolic Disorders. *Mol Cells*. , **43**(8), 686–693.

18. **Choi, A. M., Ryter, S. W. and Levine, B.** (2013). Autophagy in human health and disease. *N Engl J Med*., **368**(7), 651–662.

19. **Ohsumi Y** (2014) Historical landmarks of autophagy research. Cell Res., **24**(1), 9–23.

20. Ungermann, C. and Reggiori, F. (2018). Atg9 proteins, not so different after all. *Autophagy*, 14(8), 1456–1459.

21. **Reggiori, F., Tucker, K. A., Stromhaug, P. E. and Klionsky, D. J.** (2004). The Atg1-Atg13 complex regulates Atg9 and Atg23 retrieval transport from the pre-autophagosomal structure. *Dev Cell*. ll, **6**(1), 79–90.

22. **Araki, Y., Ku, W. C., Akioka, M., May, A. I., Hayashi, Y., Arisaka, F., Ishihama, Y. and Ohsumi, Y.** (2013). Atg38 is required for autophagy-specific phosphatidylinositol 3-kinase complex integrity. *J Cell Biol*. , **203**(2), 299–313.

23. **Kihara, A., Noda, T., Ishihara, N. and Ohsumi, Y.** (2001). Two distinct Vps34 phosphatidylinositol 3-kinase complexes function in autophagy and carboxypeptidase Y sorting in Saccharomyces cerevisiae. *J Cell Biol*., **152**(3), 519–530.

24. **Watanabe, Y., Kobayashi, T., Yamamoto, H., Hoshida, H., Akada, R., Inagaki, F., Ohsumi, Y. and Noda, N. N.** (2012). Structure-based analyses reveal distinct binding sites for Atg2 and phosphoinositides in Atg18. *J Biol Chem*., **287**(38), 31681–31690.

25. **Kotani, T., Kirisako, H., Koizumi, M., Ohsumi, Y. and Nakatogawa, H.** (2018). The Atg2-Atg18 complex tethers pre-autophagosomal membranes to the endoplasmic reticulum for autophagosome formation. *Proc Natl Acad Sci U S A*., **115**(41), 10363–10368.

26. **Ichimura, Y., Kirisako, T., Takao, T., Satomi, Y., Shimonishi, Y., Ishihara, N., Mizushima, N., Tanida, I., Kominami, E., Ohsumi, M. et al.** (2000). A ubiquitin-like system mediates protein lipidation. *Nature*, **408**(6811), 488–492.

27. **Mizushima, N., Noda, T., Yoshimori, T., Tanaka, Y., Ishii, T., George, M. D., Klionsky, D. J., Ohsumi, M. and Ohsumi, Y.** (1998). A protein conjugation system essential for autophagy. *Nature*, **395**(6700), 395–398.

28. **Kirisako, T., Ichimura, Y., Okada, H., Kabeya, Y., Mizushima, N., Yoshimori, T., Ohsumi, M., Takao, T., Noda, T. and Ohsumi, Y.** (2000). The reversible modification regulates the membrane-binding state of Apg8/Aut7 essential for autophagy and the cytoplasm to vacuole targeting pathway. *J Cell Biol*, **151**(2), 263–276.

29. **Choudhary, V., Ojha, N., Golden, A. and Prinz, W. A.** (2015). A conserved family of proteins facilitates nascent lipid droplet budding from the ER. *J Cell Biol.*, **211**(2), 261–271.

30. **Jacquier, N., Choudhary, V., Mari, M., Toulmay, A., Reggiori, F. and Schneiter, R.** (2011). Lipid droplets are functionally connected to the endoplasmic reticulum in Saccharomyces cerevisiae. *J Cell Sci*., **124**(Pt 14), 2424–2437.

31. **Kassan, A., Herms, A., Fernández-Vidal, A., Bosch, M., Schieber, N. L., Reddy, B. J., Fajardo, A., Gelabert-Baldrich, M., Tebar, F., Enrich, C., et al.** (2013). Acyl-CoA synthetase 3 promotes lipid droplet biogenesis in ER microdomains. *J Cell Biol*. , **203**(6), 985–1001.

32. **Buhman, K. K., Chen, H. C. and Farese, R. V., Jr** (2001). The enzymes of neutral lipid synthesis. *J Biol Chem*., **276**(44), 40369–40372.

33. **Cases, S., Novak, S., Zheng, Y. W., Myers, H. M., Lear, S. R., Sande, E., Welch, C. B., Lusis, A. J., Spencer, T. A., Krause, B. R et al.** (1998). ACAT-2, a second mammalian acyl-CoA: cholesterol acyltransferase. Its cloning, expression, and characterization. *J Biol Chem*. , **273**(41), 26755–26764.

34. **Cases, S., Smith, S. J., Zheng, Y. W., Myers, H. M., Lear, S. R., Sande, E., Novak, S., Collins, C., Welch, C. B., Lusis, A. J., et al.** (1998). Identification of a gene encoding an acyl CoA: diacylglycerol acyltransferase, a key enzyme in triacylglycerol synthesis. *Proc Natl Acad Sci U S A*., **95**(22), 13018–13023.

35. **Lardizabal, K. D., Mai, J. T., Wagner, N. W., Wyrick, A., Voelker, T. and Hawkins, D. J.** (2001). DGAT2 is a new diacylglycerol acyltransferase gene family: purification, cloning, and expression in insect cells of two polypeptides from Mortierella ramanniana with diacylglycerol acyltransferase activity. *J Biol Chem*., **276**(42), 38862–38869.

36. **Yang, H., Bard, M., Bruner, D. A., Gleeson, A., Deckelbaum, R. J., Aljinovic, G., Pohl, T. M., Rothstein, R. and Sturley, S. L.** (1996). Sterol esterification in yeast: a two-gene process. *Science*. **272**(5266), 1353–1356.

37. **Anderson, R. A., Joyce, C., Davis, M., Reagan, J. W., Clark, M., Shelness, G. S. and Rudel, L. L.** (1998). Identification of a form of acyl-CoA:cholesterol acyltransferase specific to liver and intestine in nonhuman primates. *J Biol Chem*, **273**(41), 26747–26754.

38. **Chang, C. C., Huh, H. Y., Cadigan, K. M. and Chang, T. Y.** (1993). Molecular cloning and functional expression of human acyl-coenzyme A:cholesterol acyltransferase cDNA in mutant Chinese hamster ovary cells. *J Biol Chem*., **268**(28), 20747–20755.

39. **Oelkers, P., Behari, A., Cromley, D., Billheimer, J. T. and Sturley, S. L.** (1998). Characterization of two human genes encoding acyl coenzyme A:cholesterol acyltransferase-related enzymes. *J Biol Chem.*, **273**(41), 26765–26771.

40. **McNeil, B. A., and Stuart, D. T.** (2018). Optimization of C16 and C18 fatty alcohol production by an engineered strain of *Lipomyces starkeyi*. *J Ind Microbiol Biotechnol.,* **45**(1), 1–14.

41. **Papanikolaou S. and Aggelis G.** (2011) Lipids of oleaginous yeasts. Part I: Biochemistry of single cell oil production. *Eur. J. Lipid Sci. Technol.*, **113**:1031–1051.

42. **Takaku, H., Matsuzawa, T., Yaoi, K., and Yamazaki, H.** (2020). Lipid metabolism of the oleaginous yeast *Lipomyces starkeyi*. *Appl Microbiol Biotechnol.*, **104**(14), 6141–6148.

43. **Miao Z., Tian X., Liang W., He Y., and Wang G.** (2020) Bioconversion of corncob hydrolysate into microbial lipid by an oleaginous yeast *Rhodotorula taiwanensis* AM2352 for biodiesel production. *Renew. Energy*. **161**:91–97.

44. **Wang, J., Ledesma-Amaro, R., Wei, Y., Ji, B. and Ji, X. J.** (2020). Metabolic engineering for increased lipid accumulation in *Yarrowia lipolytica* - A Review. *Bioresour Technol*., **313**, 123707.

45. **Takaku, H., Ebina, S., Kasuga, K., Sato, R., Ara, S., Kazama, H., Matsuzawa, T., Yaoi, K., Araki, H., Shida, Y., and et al.** (2021). Isolation and characterization of *Lipomyces starkeyi* mutants with greatly increased lipid productivity following UV irradiation. *J Biosci Bioeng.*, **131**(6), 613–621.

46. **Wang C. W.** (2016). Lipid droplets, lipophagy, and beyond. *Biochim Biophys Acta*., **1861**(8 Pt B), 793–805.

47. **Schulze, R. J., Sathyanarayan, A. and Mashek, D. G.** (2017). Breaking fat: The regulation and mechanisms of lipophagy. Biochimica et biophysica acta. *Biochim Biophys Acta Mol Cell Biol Lipids*., **1862**(10 Pt B), 1178–1187.

48. **Zechner, R., Madeo, F. and Kratky, D.** (2017). Cytosolic lipolysis and lipophagy: two sides of the same coin. *Nat Rev Mol Cell Biol*., **18**(11), 671–684.

49. **Zhang, S., Peng, X., Yang, S., Li, X., Huang, M., Wei, S., Liu, J., He, G., Zheng, H., Yang, L., et al.** (2022). The regulation, function, and role of lipophagy, a form of selective autophagy, in metabolic disorders. *Cell Death Dis*., **13**(2), 132.

50. **Han, Y. H., He, X. M., Jin, M. H., Sun, H. N., and Kwon, T.** (2023). Lipophagy: A potential therapeutic target for nonalcoholic and alcoholic fatty liver disease. *Biochem Biophys Res Commun.*, **672**, 36–44.

51.**Ouimet, M., Franklin, V., Mak, E., Liao, X., Tabas, I. and Marcel, Y. L.** (2011). Autophagy regulates cholesterol efflux from macrophage foam cells via lysosomal acid lipase. *Cell Metab*., **13**, 655–667.

52. **Singh, R., Kaushik, S., Wang, Y., Xiang, Y., Novak, I., Komatsu, M., Tanaka, K., Cuervo, A. M., and Czaja, M. J.** (2009). Autophagy regulates lipid metabolism. *Nature*, **458**, 1131–1135.

53. **Chen, K., Yuan, R., Zhang, Y., Geng, S. and Li, L.** (2017). Tollip deficiency alters atherosclerosis and steatosis by disrupting lipophagy. *J Am Heart Assoc*., **6**(4) .**Choi, A. M., Ryter, S. W. and Levine, B.** (2013). Autophagy in human health and disease. *N Engl J Med*., **368**(7), 651–662.

54. **Robichaud, S., Fairman, G., Vijithakumar, V., Mak, E., Cook, D. P., Pelletier, A. R., Huard, S., Vanderhyden, B. C., Figeys, D., Lavallée-Adam, et al.** (2021). Identification of novel lipid droplet factors that regulate lipophagy and cholesterol efflux in macrophage foam cells. *Autophagy*, **17**, 1–19.

55. **Schulze, R. J., Krueger, E. W., Weller, S. G., Johnson, K. M., Casey, C. A., Schott, M. B. and McNiven, M. A.** (2020). Direct lysosome-based autophagy of lipid droplets in hepatocytes. *Proc Natl Acad Sci U S A*., **117**(51), 32443–32452.

56. **Garcia, E. J., Liao, P. C., Tan, G., Vevea, J. D., Sing, C. N., Tsang, C. A., McCaffery, J. M., Boldogh, I. R. and Pon, L. A.** (2020). Membrane dynamics and protein targets of lipid droplet microautophagy during ER stress-induced proteostasis in the budding yeast, *Saccharomyces cerevisiae*. *Autophagy*, **17**, 1–21.

57. **Seo, A. Y., Lau, P. W., Feliciano, D., Sengupta, P., Le Gros, M. A., Cinquin, B., Larabell, C. A. and Lippincott-Schwartz, J.** (2017). AMPK and vacuole-associated Atg14p orchestrate μ-lipophagy for energy production and long-term survival under glucose starvation. *ELife*, **6**, e21690.

58. **Tsuji, T., Fujimoto, M., Tatematsu, T., Cheng, J., Orii, M., Takatori, S. and Fujimoto, T.** (2017). Niemann-Pick type C proteins promote microautophagy by expanding raft-like membrane domains in the yeast vacuole. *ELife*, **6**, e25960.

59. **Van Zutphen, T., Todde, V., De Boer, R., Kreim, M., Hofbauer, H. F., Wolinski, H., Veenhuis, M., Van Der Klei, I. J. and Kohlwein, S. D.** (2014). Lipid droplet autophagy in the yeast *Saccharomyces cerevisiae*. *Mol Biol Cell*., **25**, 290–301.

60. **Vevea, J. D., Garcia, E. J., Chan, R. B., Zhou, B., Schultz, M., Di Paolo, G., McCaffery, J. M. and Pon, L. A.** (2015). Role for lipid droplet biogenesis and microlipophagy in adaptation to lipid imbalance in yeast. *Dev Cell*, **35**, 584–599.

61. **Wang, C. W., Miao, Y. H., & Chang, Y. S.** (2014). A sterol-enriched vacuolar microdomain mediates stationary phase lipophagy in budding yeast. *J Cell Biol*, **206**, 357–366.

62. **Singh, R., Xiang, Y., Wang, Y., Baikati, K., Cuervo, A. M., Luu, Y. K., Tang, Y., Pessin, J. E., Schwartz, G. J. and Czaja, M. J.** (2009). Autophagy regulates adipose mass and differentiation in mice. *J Clin Invest*., **119**(11), 3329–3339.

63. **Yang, L., Li, P., Fu, S., Calay, E. S. and Hotamisligil, G. S.** (2010). Defective hepatic autophagy in obesity promotes ER stress and causes insulin resistance. *Cell Metab*., **11**(6), 467–478.

64. **Kurat, C. F., Wolinski, H., Petschnigg, J., Kaluarachchi, S., Andrews, B., Natter, K. and Kohlwein, S. D.** (2009). Cdk1/Cdc28-dependent activation of the major triacylglycerol lipase Tgl4 in yeast links lipolysis to cell-cycle progression. *Mol Cell*. , **33**(1), 53–63.

65. **Epple, U. D., Suriapranata, I., Eskelinen, E. L. and Thumm, M.** (2001). Aut5/Cvt17p, a putative lipase essential for disintegration of autophagic bodies inside the vacuole. *J Bacteriol*., **183**(20), 5942–5955.

66. **Teter, S. A., Eggerton, K. P., Scott, S. V., Kim, J., Fischer, A. M. and Klionsky, D. J.** (2001). Degradation of lipid vesicles in the yeast vacuole requires function of Cvt17, a putative lipase. *J Biol Chem*., **276**(3), 2083–2087.

67. **Shibata, M., Yoshimura, K., Furuya, N., Koike, M., Ueno, T., Komatsu, M., Arai, H., Tanaka, K., Kominami, E., et al.** (2009). The MAP1-LC3 conjugation system is involved in lipid droplet formation. *Biochem Biophys Res Commun*., **382**(2), 419–423.

68. **Shibata, M., Yoshimura, K., Tamura, H., Ueno, T., Nishimura, T., Inoue, T., Sasaki, M., Koike, M., Arai, H., Kominami, E., et al.** (2010). LC3, a microtubule-associated protein1A/B light chain3, is involved in cytoplasmic lipid droplet formation. *Biochem Biophys Res Commun*., **393**(2), 274–279.

69. **Maeda, Y., Oku, M. and Sakai, Y.** (2017). Autophagy-independent function of Atg8 in lipid droplet dynamics in yeast. *J Biochem*., **161**(4), 339–348.

70. **Robenek, H., Hofnagel, O., Buers, I., Robenek, M. J., Troyer, D. and Severs, N. J.** (2006). Adipophilin-enriched domains in the ER membrane are sites of lipid droplet biogenesis. *J Cell Sci*., **119**(Pt 20), 4215–4224.

71. **Wilfling, F., Wang, H., Haas, J. T., Krahmer, N., Gould, T. J., Uchida, A., Cheng, J. X., Graham, M., Christiano, R., Fröhlich, F. et al.** (2013). Triacylglycerol synthesis enzymes mediate lipid droplet growth by relocalizing from the ER to lipid droplets. *Dev Cell*., **24**(4), 384–399.

72. **Binns, D., Januszewski, T., Chen, Y., Hill, J., Markin, V. S., Zhao, Y., Gilpin, C., Chapman, K. D., Anderson, R. G. and Goodman, J. M.** (2006). An intimate collaboration between peroxisomes and lipid bodies. *J Cell Biol*., **173**(5), 719–731.

73. **Wang, H., Lei, M., Hsia, R. C. and Sztalryd, C.** (2013). Analysis of lipid droplets in cardiac muscle. *Methods Cell Biol*., **116**, 129–149.

74. **Zhang, H., Wang, Y., Li, J., Yu, J., Pu, J., Li, L., Zhang, H., Zhang, S., Peng, G., Yang, F. and Liu, P.** (2011). Proteome of skeletal muscle lipid droplet reveals association with mitochondria and apolipoprotein a-I. *J Proteome Res*. , **10**(10), 4757–4768.

75. **Pu, J., Ha, C. W., Zhang, S., Jung, J. P., Huh, W. K. and Liu, P.** (2011). Interactomic study on interaction between lipid droplets and mitochondria. *Protein Cell*., **2**(6), 487–496.

76. **Yu, J., Zhang, S., Cui, L., Wang, W., Na, H., Zhu, X., Li, L., Xu, G., Yang, F., Christian, M., et al.** (2015). Lipid droplet remodeling and interaction with mitochondria in mouse brown adipose tissue during cold treatment. *Biochim. Biophys. Acta*, **1853**(5), 918–928.

77. **Benador, I. Y., Veliova, M., Liesa, M., and Shirihai, O. S.** (2019). Mitochondria Bound to Lipid Droplets: Where Mitochondrial Dynamics Regulate Lipid Storage and Utilization. *Cell Metab.*, **29**(4), 827–835.

78. **McBride, H. M., Neuspiel, M., and Wasiak, S.** (2006). Mitochondria: more than just a powerhouse. *Curr Biol*., **16**(14), R551–R560.

79. **Suen, D. F., Norris, K. L. and Youle, R. J.** (2008). Mitochondrial dynamics and apoptosis. *Genes Dev*., **22**(12), 1577–1590.

80. **Bock, F. J. and Tait, S. W. G.** (2020). Mitochondria as multifaceted regulators of cell death. *Nat Rev Mol Cell Biol.*, **21**(2), 85–100.

81. **Dard, L., Blanchard, W., Hubert, C., Lacombe, D. and Rossignol, R.** (2020). Mitochondrial functions and rare diseases. *Mol Aspects Med*., **71**, 100842.

82. **Herms, A., Bosch, M., Reddy, B. J., Schieber, N. L., Fajardo, A., Rupérez, C., Fernández-Vidal, A., Ferguson, C., Rentero, C., Tebar, F., Enrich, C., Parton, R. G., Gross, S. P., and Pol, A**. (2015). AMPK activation promotes lipid droplet dispersion on detyrosinated microtubules to increase mitochondrial fatty acid oxidation. *Nat Commun.*, **6**, 7176.

83. **Nguyen, T. B., Louie, S. M., Daniele, J. R., Tran, Q., Dillin, A., Zoncu, R., Nomura, D. K., and Olzmann, J. A.** (2017). DGAT1-Dependent Lipid Droplet Biogenesis Protects Mitochondrial Function during Starvation-Induced Autophagy. *Dev Cell.*, **42**(1), 9–21.e5.

84. **Rambold, A. S., Cohen, S. and Lippincott-Schwartz, J.** (2015). Fatty acid trafficking in starved cells: regulation by lipid droplet lipolysis, autophagy, and mitochondrial fusion dynamics. *Dev Cell.*, **32**(6), 678–692.

85. **Benador, I. Y., Veliova, M., Mahdaviani, K., Petcherski, A., Wikstrom, J. D., Assali, E. A., Acín-Pérez, R., Shum, M., Oliveira, M. F., Cinti, S., et al.** (2018). Mitochondria

Bound to Lipid Droplets Have Unique Bioenergetics, Composition, and Dynamics that Support Lipid Droplet Expansion. Cell Metab., **27**(4), 869–885.e6.

86. **Peute, J., van der Gaag, M. A. and Lambert, J. G.** (1978). Ultrastructure and lipid content of the liver of the zebrafish, Brachydanio rerio, related to vitellogenin synthesis. *Cell Tissue Res.*, **186**(2), 297–308.

87. **Mottillo, E. P., Balasubramanian, P., Lee, Y. H., Weng, C., Kershaw, E. E., and Granneman, J. G.** (2014). Coupling of lipolysis and de novo lipogenesis in brown, beige, and white adipose tissues during chronic β3-adrenergic receptor activation. *J Lipid Res*., **55**(11), 2276–2286.

88. **O'Sullivan, D., van der Windt, G. J., Huang, S. C., Curtis, J. D., Chang, C. H., Buck, M. D., Qiu, J., Smith, A. M., Lam, W. Y., et al.** (2014). Memory CD8(+) T cells use cell-intrinsic lipolysis to support the metabolic programming necessary for development. *Immunity*, **41**(1), 75–88.

89. **Sanchez-Gurmaches, J., Tang, Y., Jespersen, N. Z., Wallace, M., Martinez Calejman, C., Gujja, S., Li, H., Edwards, Y., Wolfrum, C., Metallo, C. M., et al.** (2018). Brown Fat AKT2 Is a Cold-Induced Kinase that Stimulates ChREBP-Mediated De Novo Lipogenesis to Optimize Fuel Storage and Thermogenesis. *Cell Metab*., **27**(1), 195–209.e6.

90. **McGarry, J. D., Meier, J. M., and Foster, D. W.** (1973). The effects of starvation and refeeding on carbohydrate and lipid metabolism in vivo and in the perfused rat liver. The relationship between fatty acid oxidation and esterification in the regulation of ketogenesis. *J Biol Chem*, **248**(1), 270–278.

91. **McGarry, J. D., Mannaerts, G. P., and Foster, D. W.** (1978). Characteristics of fatty acid oxidation in rat liver homogenates and the inhibitory effect of malonyl-CoA. *Biochim Biophys Acta.*, **530**(3), 305–313.

92. **Veliova, M., Petcherski, A., Liesa, M., & Shirihai, O. S.** (2020). The biology of lipid droplet-bound mitochondria. *Semin Cell Dev Biol*., **108**, 55–64.

93. **Kornmann, B., Currie, E., Collins, S. R., Schuldiner, M., Nunnari, J., Weissman, J. S. and Walter, P.** (2009). An ER-mitochondria tethering complex revealed by a synthetic biology screen. *Science*, **325**(5939), 477–481.

94. **John Peter, A. T., Herrmann, B., Antunes, D., Rapaport, D., Dimmer, K. S. and Kornmann, B.** (2017). Vps13-Mcp1 interact at vacuole-mitochondria interfaces and bypass ER-mitochondria contact sites. *J Cell Biol*, **216**(10), 3219–3229.

95. **Joshi A. S.** (2021). Peroxisomal Membrane Contact Sites in Yeasts. *Front Cell Dev Biol*., **9**, 735031.

96. **Shai, N., Yifrach, E., van Roermund, C. W. T., Cohen, N., Bibi, C., IJlst, L., Cavellini, L., Meurisse, J., Schuster, R., Zada, L. et al.** 2018) Systematic mapping of contact sites reveals tethers and a function for the peroxisome-mitochondria contact. *Nat. Commun.,* **9**(1), 1761.

97. **Murphy M. P.** (2009). How mitochondria produce reactive oxygen species. *Biochem J*., **417**(1), 1–13.

98. **Kirkinezos, I. G. and Moraes, C. T.** (2001). Reactive oxygen species and mitochondrial diseases. *Semin Cell Dev Biol*., **12**(6), 449–457.

99. **Doblado, L., Lueck, C., Rey, C., Samhan-Arias, A. K., Prieto, I., Stacchiotti, A. and Monsalve, M.** (2021). Mitophagy in Human Diseases. *Int J Mol Sci*., **22**(8), 3903.

100. **Onishi, M. and Okamoto, K.** (2021). Mitochondrial clearance: Mechanisms and roles in cellular fitness. *FEBS Lett*., **595**(8), 1239–1263.

101. **Onishi, M., Yamano, K., Sato, M., Matsuda, N. and Okamoto, K.** (2021). Molecular mechanisms and physiological functions of mitophagy. *EMBO J*., **40**(3), e104705.

102. **Okamoto, K., Kondo-Okamoto, N. and Ohsumi, Y.** (2009). Mitochondria-anchored receptor Atg32 mediates degradation of mitochondria via selective autophagy. *Dev Cell.*, **17**(1), 87–97.

103. **Kanki, T., Wang, K., Cao, Y., Baba, M. and Klionsky, D. J.** (2009). Atg32 is a mitochondrial protein that confers selectivity during mitophagy. *Dev Cell*. , **17**(1), 98–109.

104. **Kanki, T., Kurihara, Y., Jin, X., Goda, T., Ono, Y., Aihara, M., Hirota, Y., Saigusa, T., Aoki, Y., Uchiumi, T. and Kang, D.** (2013). Casein kinase 2 is essential for mitophagy. *EMBO Rep*, **14**(9), 788–794.

105. **Furukawa, K., Fukuda, T., Yamashita, S. I., Saigusa, T., Kurihara, Y., Yoshida, Y., Kirisako, H., Nakatogawa, H. and Kanki, T.** (2018). The PP2A-like Protein Phosphatase Ppg1 and the Far Complex Cooperatively Counteract CK2-Mediated Phosphorylation of Atg32 to Inhibit Mitophagy. *Cell Rep*., **23**(12), 3579–3590.

106. **Richard, V. R., Leonov, A., Beach, A., Burstein, M. T., Koupaki, O., Gomez-Perez, A., Levy, S., Pluska, L., Mattie, S., Rafesh, RH. et al.** (2013). Macromitophagy is a longevity assurance process that in chronologically aging yeast limited in calorie supply sustains functional mitochondria and maintains cellular lipid homeostasis. *Aging*, **5**(4), 234–269.

107. **Yau, W. W., Wong, K. A., Zhou, J., Thimmukonda, N. K., Wu, Y., Bay, B. H., Singh, B. K., & Yen, P. M.** (2021). Chronic cold exposure induces autophagy to promote fatty acid oxidation, mitochondrial turnover, and thermogenesis in brown adipose tissue. *iScience*, **24**(5), 102434.

108. **Fu, T., Xu, Z., Liu, L., Guo, Q., Wu, H., Liang, X., Zhou, D., Xiao, L., Liu, L., Liu, Y., et al.** (2018). Mitophagy Directs Muscle-Adipose Crosstalk to Alleviate Dietary Obesity. *Cell Rep.*, **23**(5), 1357–1372.

109. **Tong, M., Saito, T., Zhai, P., Oka, S. I., Mizushima, W., Nakamura, M., Ikeda, S., Shirakabe, A. and Sadoshima, J.** (2019). Mitophagy Is Essential for Maintaining Cardiac Function During High Fat Diet-Induced Diabetic Cardiomyopathy. *Circ Res*., **124**(9), 1360–1371.

110. **Long, M. and McWilliams, T. G.** (2023). Lipid droplets promote efficient mitophagy. *Autophagy*, **19**(2), 724–725.

111. **Giacomello, M., and Scorrano, L.** (2018). The INs and OUTs of mitofusins. *J Cell Biol.*, **217**(2), 439–440.

112. **Angerbauer, C., Siebenhofer, M., Mittelbach, M., and Guebitz, G. M.** (2008). Conversion of sewage sludge into lipids by *Lipomyces starkeyi* for biodiesel production. *Bioresour Technol.*, **99**(8), 3051–3056.

113. **Sutanto, S., Go, A.W., Chen, K.-H., Nguyen, P.L.T., Ismadji, S., Ju, Y.-H.** (2017) Release of sugar by acid hydrolysis from rice bran for single cell oil production and subsequent in-situ transesterification for biodiesel preparation Fuel Process. *Technol.*, **167**, pp. 281-291

114. **Juanssilfero, A. B., Kahar, P., Amza, R. L., Miyamoto, N., Otsuka, H., Matsumoto, H., Kihira, C., Thontowi, A., Yopi, Ogino, C., et al.** (2018). Effect of inoculum size on single-cell oil production from glucose and xylose using oleaginous yeast *Lipomyces starkeyi*. *J Biosci Bioeng.*, **125**(6), 695–702.

115. **Duan, L., and Okamoto, K.** (2021). Mitochondrial dynamics and degradation in the oleaginous yeast *Lipomyces starkeyi*. *Genes Cells*, **26**(8), 627–635.

116. **Liu, Y., and Okamoto, K.** (2021). Regulatory mechanisms of mitophagy in yeast. *Biochim Biophys Acta Gen Subj*., **1865**(5), 129858.

117. **Maruyama, T., and Noda, N. N.** (2017). Autophagy-regulating protease Atg4: structure, function, regulation and inhibition. *J Antibiot (Tokyo)*, **71**(1), 72–78. Advance online publication.

118. **Eiyama, A., and Okamoto, K.** (2017). Assays for Mitophagy in Yeast. *Methods Mol Biol.*, **1567**, 337–347.

119. **Oguro, Y., Yamazaki, H., Shida, Y., Ogasawara, W., Takagi, M. and Takaku, H.** (2015). Multicopy integration and expression of heterologous genes in the oleaginous yeast, *Lipomyces starkeyi*. *Biosci Biotechnol Biochem.*, **79**(3), 512–515.

120. **Nagumo, S., and Okamoto, K.** (2018). Investigation of Yeast Mitophagy with Fluorescence Microscopy and Western Blotting. *Methods Mol Biol*. **1759**, 71–83.

121. **Calvelli, H., Krigman, J., Onishi, M., Narendra, D. P., Sun, N. and Okamoto, K.** (2020). Detection of mitophagy in mammalian cells, mice, and yeast. *Methods Cell Biol*., **155**, 557–579.

122. **Magen, S., Seybold, H., Laloum, D., and Avin-Wittenberg, T.** (2022). Metabolism and autophagy in plants-a perfect match. *FEBS Lett*., **596**(17), 2133–2151.

123. **Todde, V., Veenhuis, M. and van der Klei, I. J.** (2009). Autophagy: principles and significance in health and disease. *Biochim Biophys Acta*., **1792**(1), 3–13.

124. **Xie, Z., Nair, U. and Klionsky, D. J.** (2008). Atg8 controls phagophore expansion during autophagosome formation. *Mol Biol Cell*., **19**(8), 3290–3298.

125. **Kirisako, T., Ichimura, Y., Okada, H., Kabeya, Y., Mizushima, N., Yoshimori, T., Ohsumi, M., Takao, T., Noda, T. and Ohsumi, Y.** (2000). The reversible modification regulates the membrane-binding state of Apg8/Aut7 essential for autophagy and the cytoplasm to vacuole targeting pathway. *J Cell Biol*, **151**(2), 263–276.

126. **Torggler, R., Papinski, D., and Kraft, C.** (2017) Assays to monitor autophagy in *Saccharomyces cerevisiae*. *Cells* 6, 23

127. **Bórquez, J.C., Díaz-Castro, F., La Fuente, F.P., Espinoza, K., Figueroa, A.M., Martínez-Ruíz, I., Hernández, V., López-Soldado, I., Ventura, R., Domingo, J.C., Bosch, M., Fajardo, A., Sebastián, D., Espinosa, A., Pol, A., Zorzano, A., Cortés, V., Hernández-Alvarez, M.I., and Troncoso, R.** (2024) Mitofusin-2 induced by exercise modifies lipid droplet-mitochondria communication, promoting fatty acid oxidation in male mice with NAFLD. *Metabolism* **152,** 155765.

128. **Takeshige, K., Baba, M., Tsuboi, S., Noda, T. and Ohsumi, Y.** (1992). Autophagy in yeast demonstrated with proteinase-deficient mutants and conditions for its induction. *J Cell Biol.*, **119**(2), 301–311.

129. **Li, D., Song, J. Z., Li, H., Shan, M. H., Liang, Y., Zhu, J. and Xie, Z.** (2015). Storage lipid synthesis is necessary for autophagy induced by nitrogen starvation. *FEBS letters*, **589**(2), 269–276.

130. **Shpilka, T., Welter, E., Borovsky, N., Amar, N., Mari, M., Reggiori, F. and Elazar, Z.** (2015). Lipid droplets and their component triglycerides and steryl esters regulate autophagosome biogenesis. *EMBO J.*, **34**(16), 2117–2131.

131. **Régnacq, M., Voisin, P., Sere, Y. Y., Wan, B., Soeroso, V. M. S., Bernard, M., Camougrand, N., Bernard, F. X., Barrault, C. and Bergès, T.** (2016). Increased fatty acid synthesis inhibits nitrogen starvation-induced autophagy in lipid droplet-deficient yeast. *Biochem Biophys Res Commun*., **477**(1), 33–39.

132. **Liang, M. H. and Jiang, J. G.** (2013). Advancing oleaginous microorgan- isms to produce lipid via metabolic engineering technology. *Prog Lipid Res.*, **52**(4), 395–408.

133. **Calvey, C.H., Willis, L.B., and Jeffries, T.W.** (2014) An optimized transformation protocol for *Lipomyces starkeyi*. *Curr. Genet*. **60**, 223–230

134. **Osumi, M., Shimoda, C., and Yanagishima, N.** (1974) Mating reaction in *Saccharomyces cerevisiae*. V. Changes in the fine structure during the mating reaction. *Arch. Mikrobiol*. **97**, 27–38

4 TABLES AND FIGURES

Table 1. Yeast strains used in this study

Name	Genotypes
KOY76	*Saccharomyces cerevisiae* BY4741 *his3Δ1 leu2Δ0 met15Δ0 ura3Δ0*
KOY1387	BY4741 *his3Δ1::TEF P -mito-DHFR-mCherry::CgHIS3*
KOY1422	BY4741 *his3Δ1::TEF P -mito-DHFR-mCherry::CgHIS3 atg32::kanMX6*
KOY5787	BY4741 *his3Δ1::TEF P -mito-DHFR-mCherry::CgHIS3 Vph1-GFP+(hph)*
KOY5789	BY4741 *his3Δ1::TEF P-mito-DHFR-mCherry::CgHIS3 Vph1-GFP+(hph) atg32::kanMX6*
KOY5837	BY4741 *his3Δ1::TDH3-mCherry::kanMX6*
KOY5870	BY4741 *his3Δ1::TDH3-mCherry::kanMX6 atg7::natNT2*
KOY7912	*Lipomyces starkeyi* NRRL Y-1388
KOY9620	*Lipomyces starkeyi* NRRL Y-1388 *P -mito-DHFR-mCherry*
KOY10042	*Lipomyces starkeyi* NRRL Y-1388 *P -AirID-AGIA-Atg8*
KOY11027	*Lipomyces starkeyi* NRRL Y-1388 *P -mito-DHFR-mCherry P-LsATG4-3V5*
KOY10206	*Lipomyces starkeyi* NRRL Y-1388 *P -Atg8-AGIA-AirID*
KOY12992	BY4741 *his3Δ1::TEF P -mito-DHFR-mCherry::CgHIS3 atg4::GPD-ATG4::natNT2*
KOY13014	BY4741 *his3Δ1::TDH3-mCherry::kanMX6CgHIS3 atg4::GPD-ATG4::natNT2*

Table 2. Plasmids used in this study

Name	Relevant characteristics
pKS-18S-hph	*541 bp upstream & 892 bp downstream 18S rDNA, 998 bp promoter & 513 bp termitator of lsTDH3 & 1026 bp hph*
pKS-18S-mito-DHFR-mCherry-hph	*541 bp upstream & 892 bp downstream 18S rDNA, 998 bp promoter & 513 bp termitator of lsTDH3, 1026 bp hph, 1497 bp mito-DHFR-mCherry, 1207 bp promoter & 520 bp termitator of lsTEF*
pBSII-TEF-mtDHFR-mCherry-CgHis	*1494 bp mito-DHFR-mCherry*
pKS-18S-LsATG4-3V5-nat	*541 bp upstream & 892 bp downstream 18S rDNA, 998 bp promoter & 513 bp termitator of lsTDH3, 573 bp nat, 1458 bp LsATG4, 136bp 3V5, 1207 bp promoter & 520 bp termitator of lsTEF*
pKS-18S-AirID-AGIA-LsATG8	*541 bp upstream & 892 bp downstream 18S rDNA, 998 bp promoter & 513 bp termitator of lsTDH3, 1026 bp hph, 357 bp LsATG8(cDNA), 957bp AirID, 30bp AGIA, 1207 bp promoter & 520 bp termitator of lsTEF*
pKS-18S- LsATG8-AGIA-AirID	*541 bp upstream & 892 bp downstream 18S rDNA, 998 bp promoter & 513 bp termitator of lsTDH3, 1026 bp hph, 357 bp LsATG8(cDNA), 957bp AirID, 30bp AGIA, 1207 bp promoter & 520 bp termitator of lsTEF*

Figures

Graphic Abstract

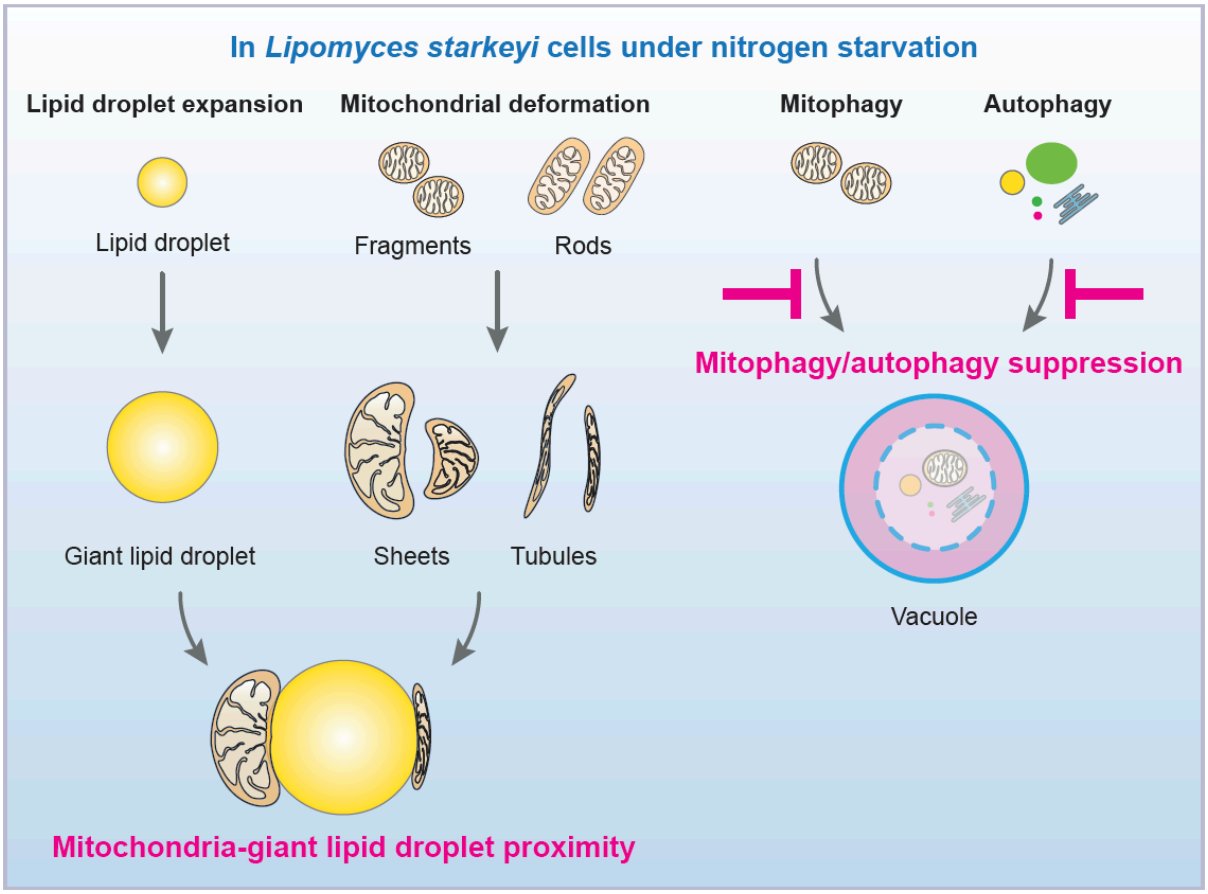

Figure 1-1

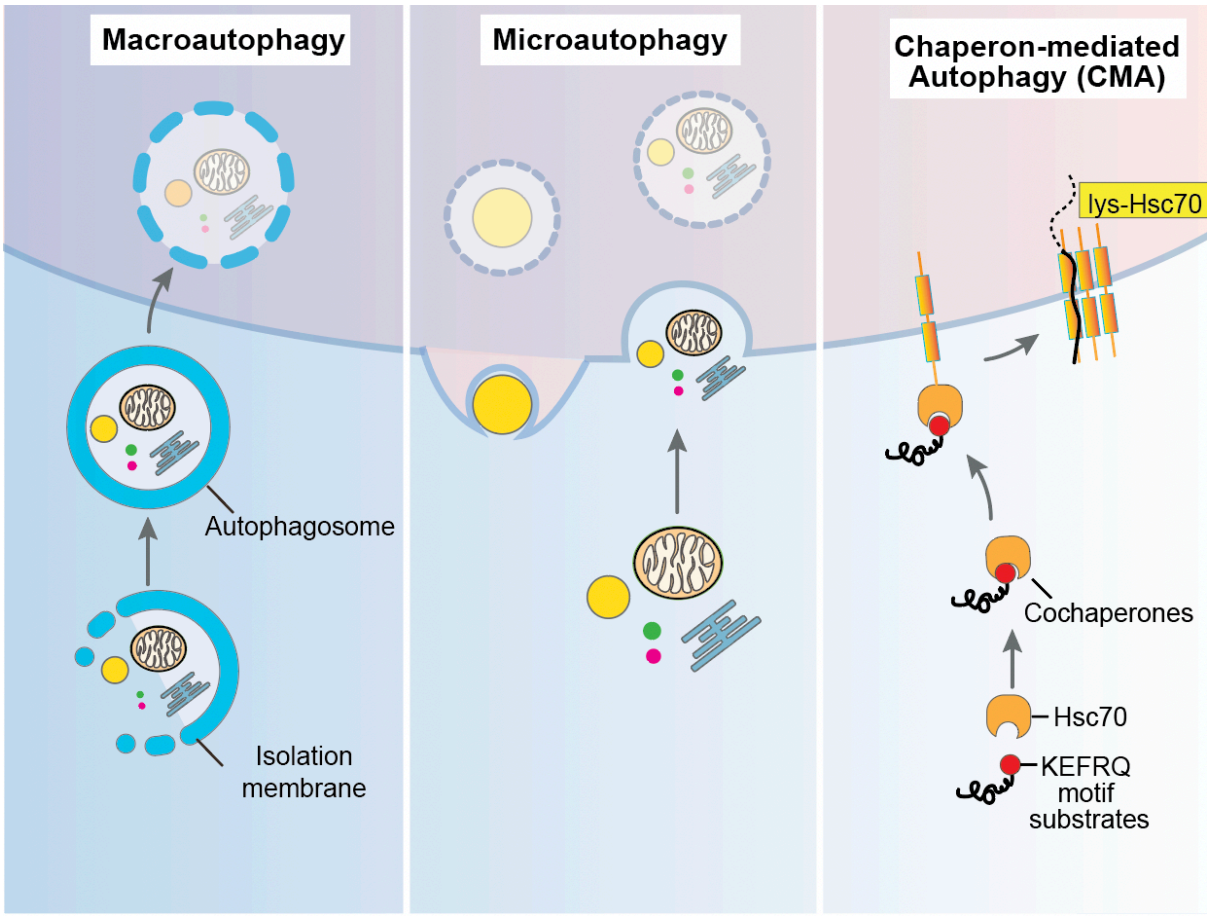

Figure 1-1 A model for three types of autophagy: Macroautophagy, Microautophagy and Chaperom-mediated autophagy.

Figure 1-2

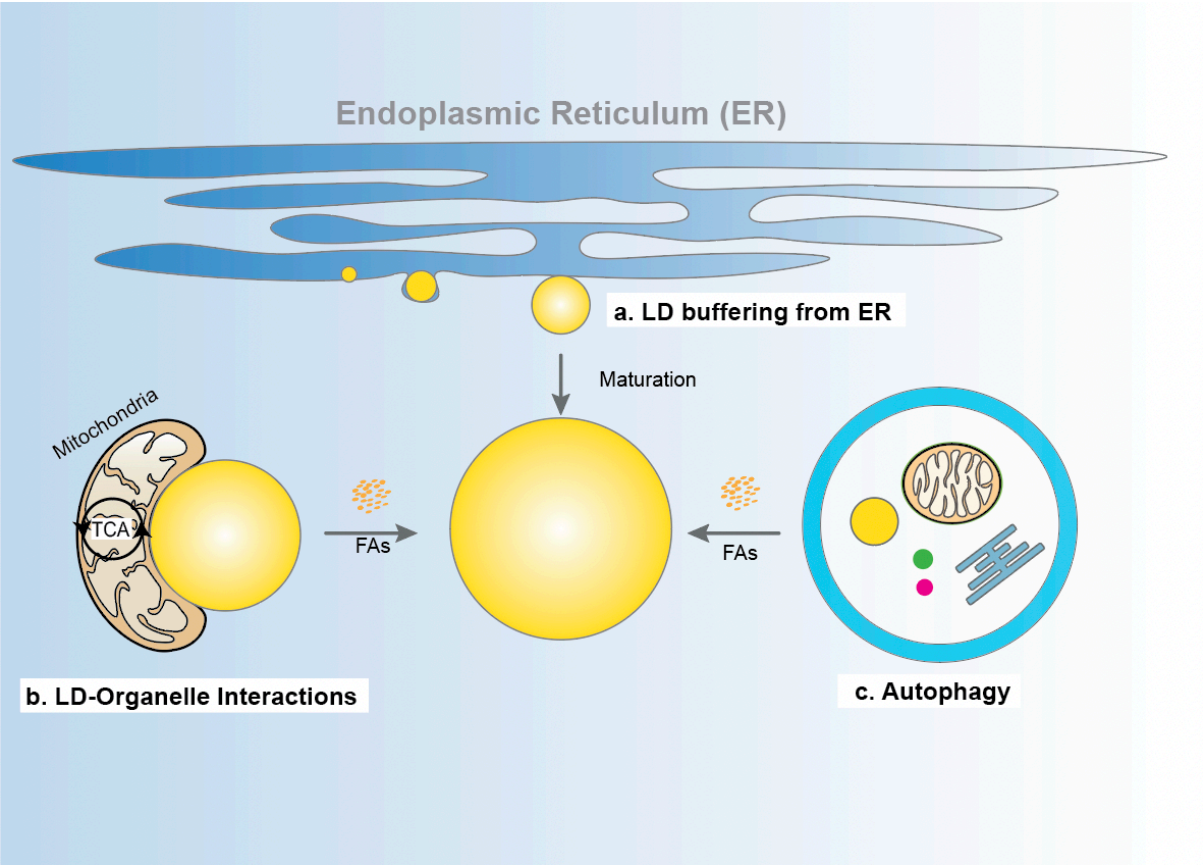

Figure 1-2 A model for LD biogenesis by a. ER buffering, b. LD-mitochondria interaction and Autophagy.

Figure 1-3 LD breakdown

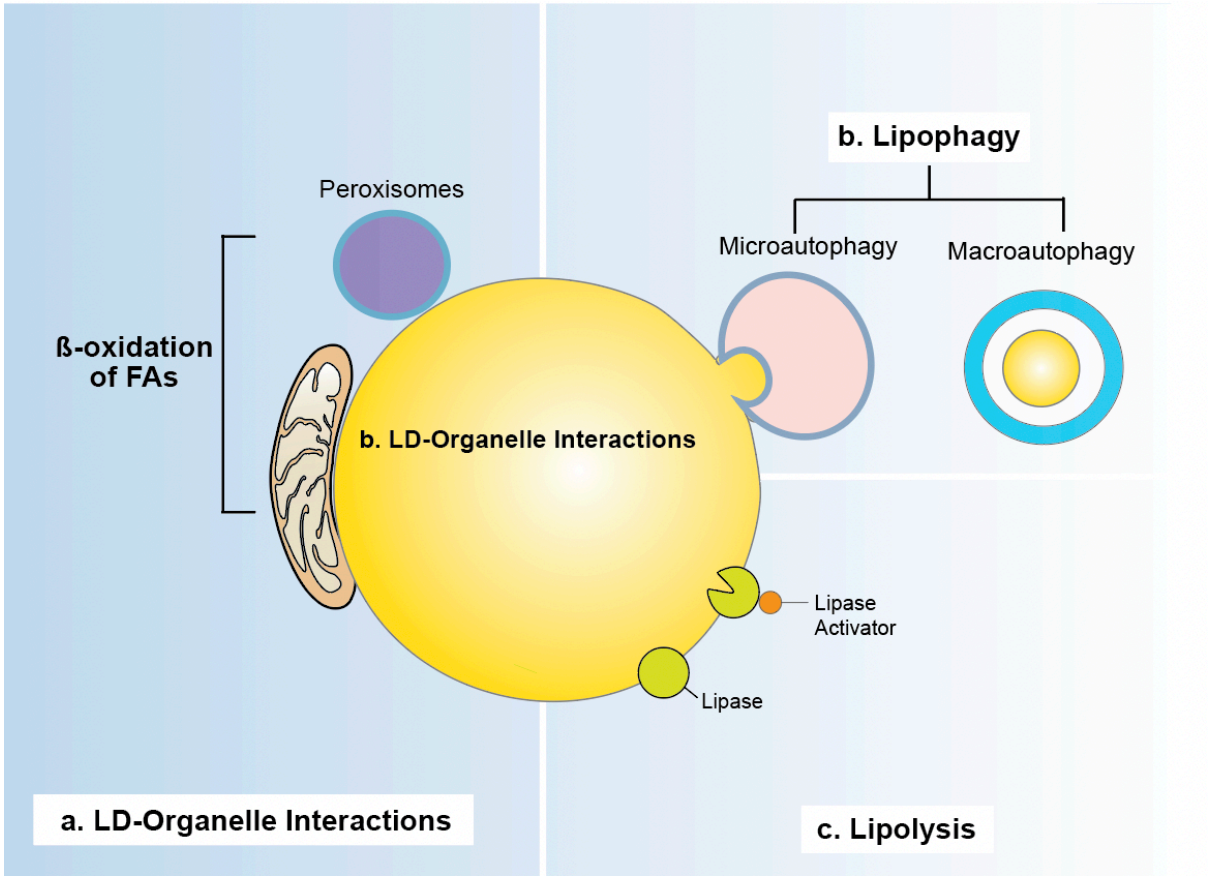

Figure 1-3 A model for LD breakdown by a. ß-oxidation in mitochondria and peroxisomes b. Lipophagy, and c. Lipolysis.

Figure 1-4

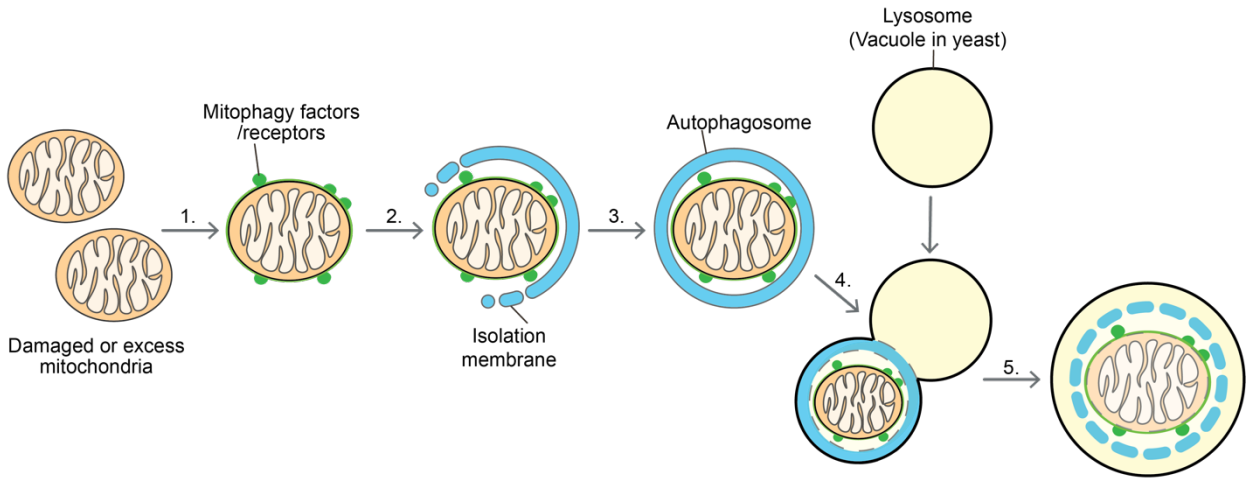

Figure 1-4. A model for mitophagy, 1. Recruitment and activation of mitophagy factors or receptors on damaged or access mitochondria. 2. Recognition by autophagy proteins and formation of isolation membrane. 3. Sequestration by autophagosome 4. Fusion with lysosome (vacuole in yeast) 5. Degradation and recycle.

Figure 1-5

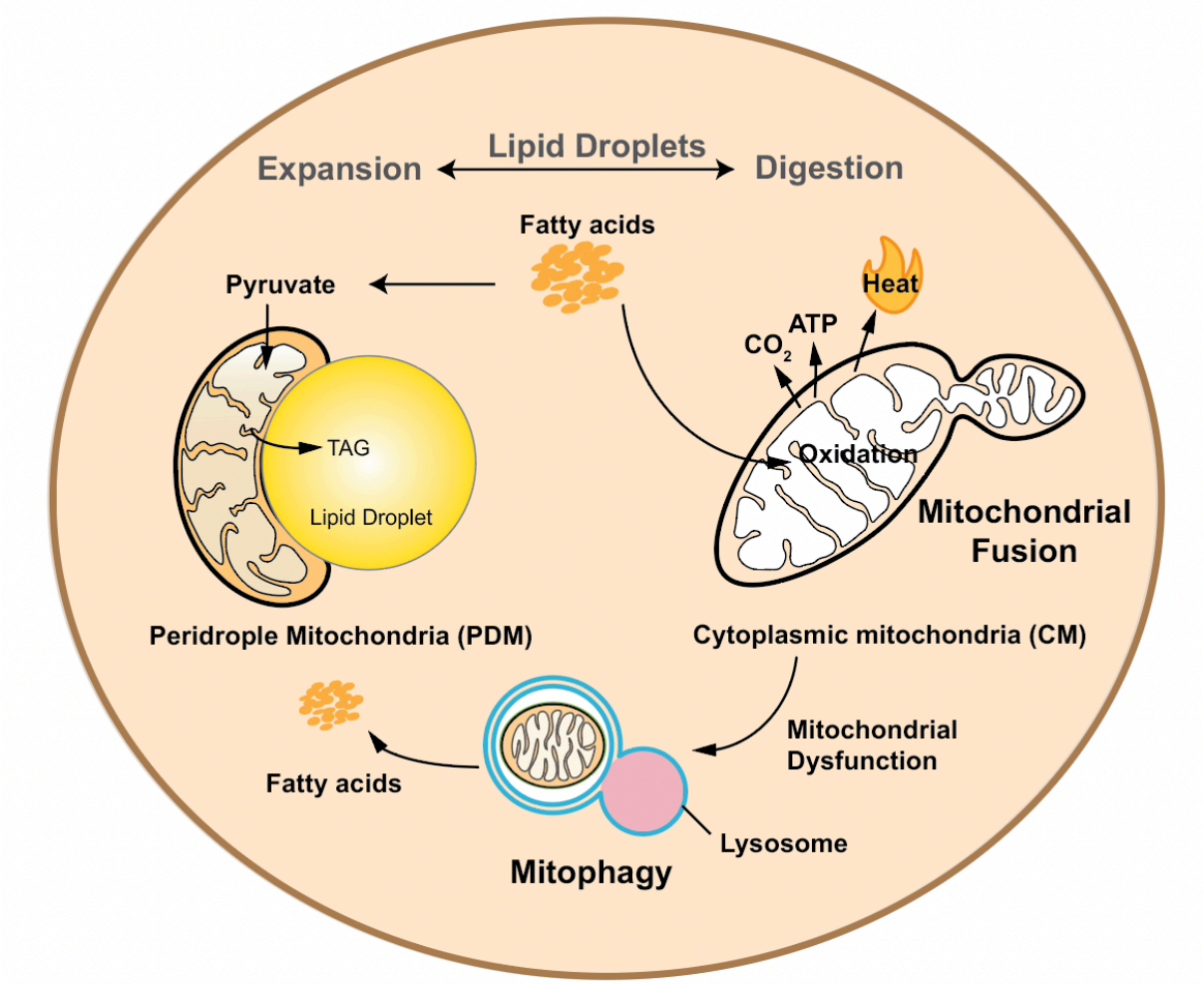

Fig 1-5 A model for introduction on mitochondrial dynamics and mitophagy during LD expansion and digestion.

Figure 2-1

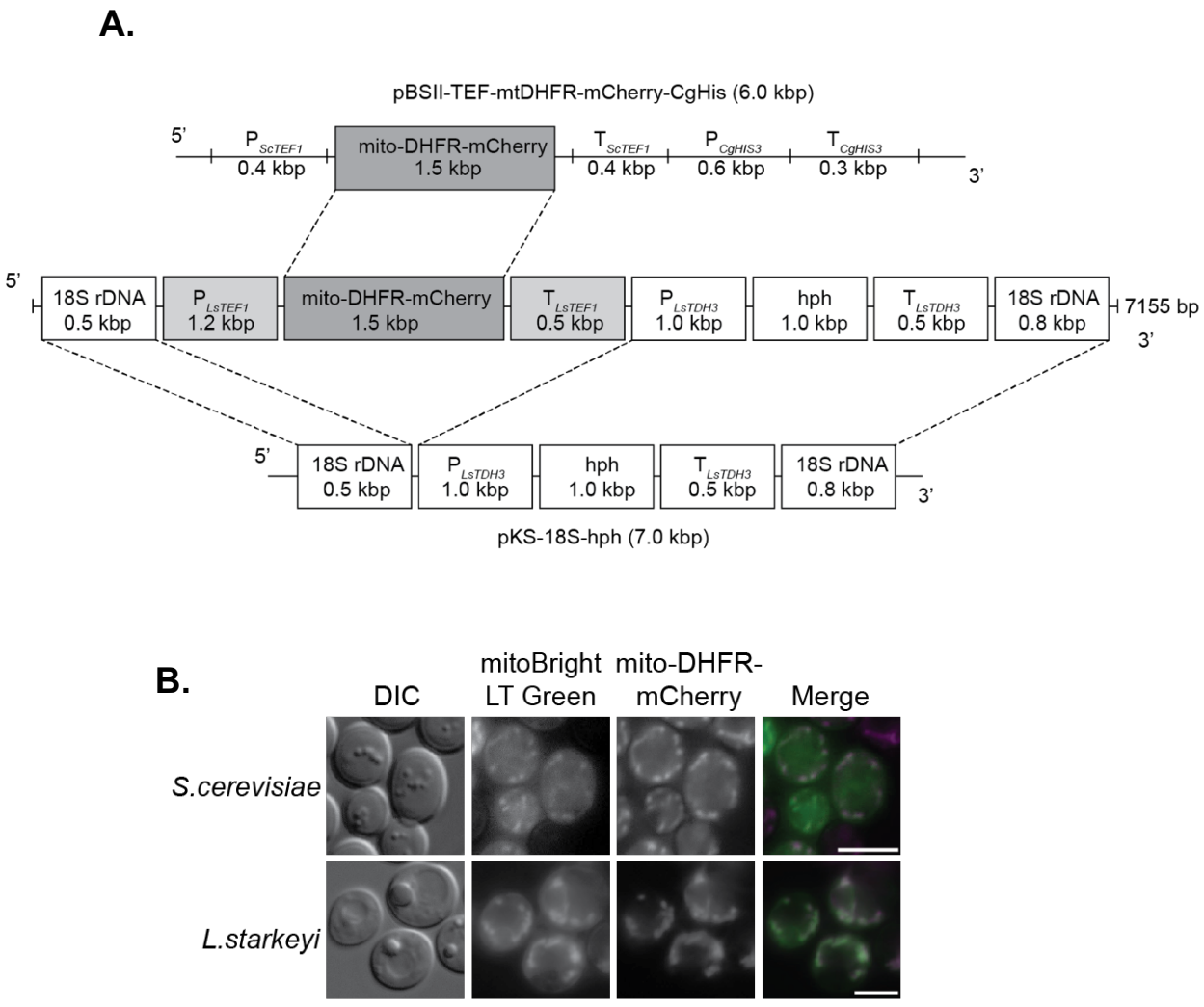

Figure 2-1. The fluorescent marker mito-DHFR-mCherry visualizes mitochondria in *L. starkeyi* cells. (A) Construction scheme of the mito-DHFR-mCherry integration cassette for *L. starkeyi.* (B) *S. cerevisiae* and *L. starkeyi* cells expressing mito-DHFR-mCherry were cultured in SDCA overnight. 1 OD_{600} units of cells were washed and suspended in 1 ml fresh SDCA, and MitoBright LT Green was added into cell suspension (final concentration = 0.1 M). Cells were then incubated in room temperature for 15 min, washed once with fresh medium, and observed under a fluorescence microscope. Scale bar, 5 μm.

C.

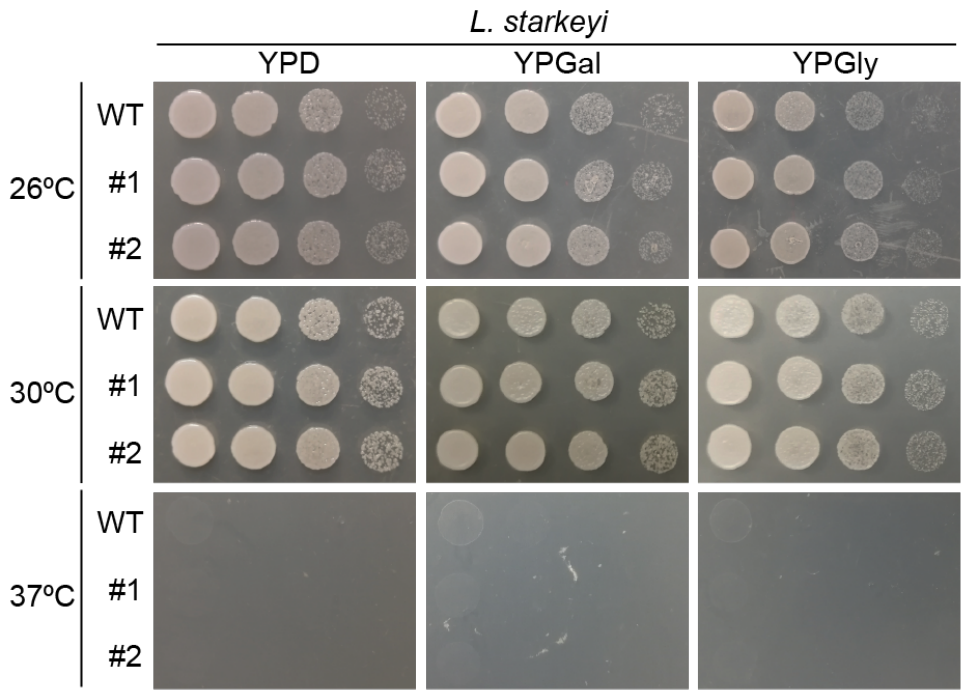

Figure 2-1. The fluorescent marker mito-DHFR-mCherry visualizes mitochondria in *L. starkeyi* cells. (C) 1 OD_{600} units of *L. starkeyi* cells were suspended in distilled water, diluted to 1:5, 1:25, and 1:125, spotted on YPD, YPGal, and YPGly plates, and incubated at 26 ℃, 30 ℃, and 37 ℃ for 2 days

Figure 2-2

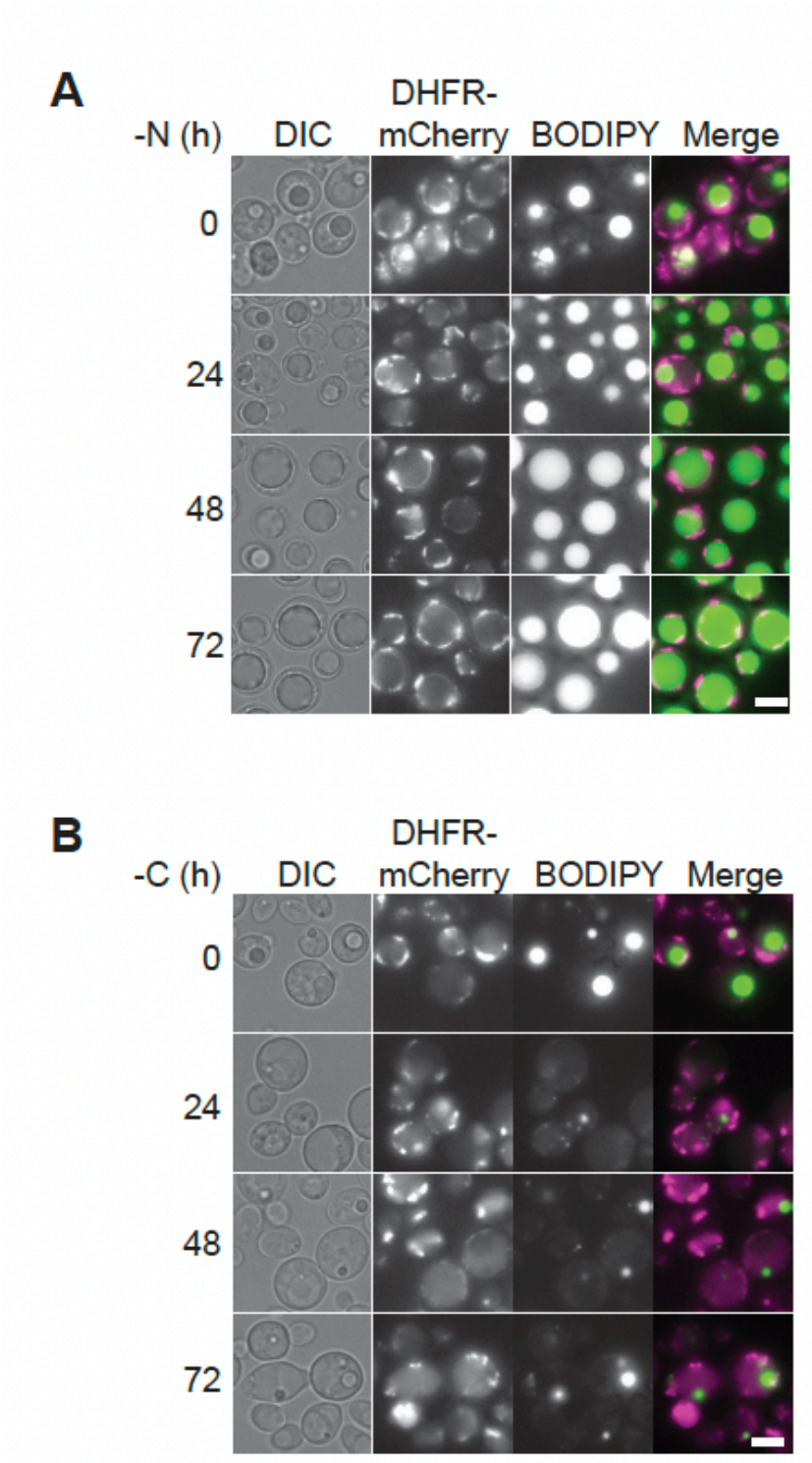

Figure 2-2 Mitochondria form tubule-like structures in nitrogen-depleted *L. starkeyi* cells. (A and B) Cells expressing mito-DHFR-mCherry were grown under nitrogen (-N) or carbon (-C) starvation. Mitochondrial shapes were analyzed at the indicated time points using a fluorescence microscope. (C) The average total area of LDs in each cell was quantified by the area of BODIPY signals. Scale bar, 5 μm.

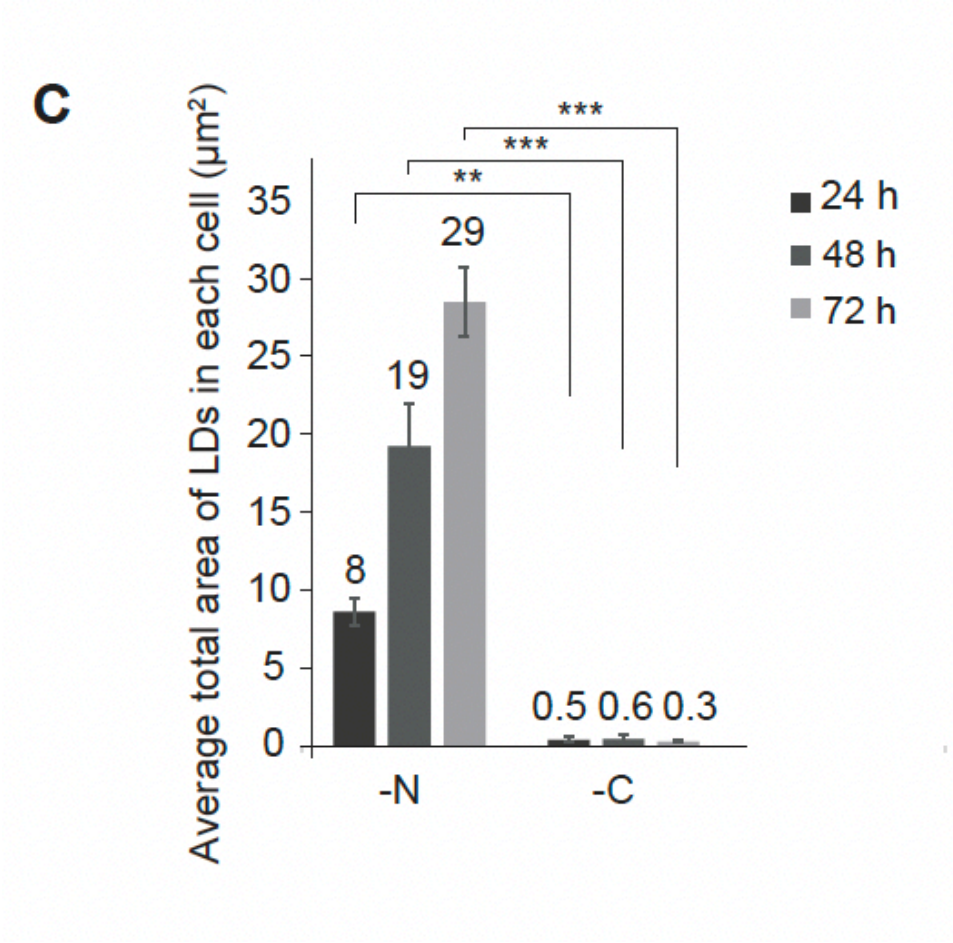

Figure 2-2 Mitochondria form tubule-like structures in nitrogen-depleted *L. starkeyi* cells. (A and B) Cells expressing mito-DHFR-mCherry were grown under nitrogen (-N) or carbon (-C) starvation. Mitochondrial shapes were analyzed at the indicated time points using a fluorescence microscope. (C) The average total area of LDs in each cell was quantified by the area of BODIPY signals. Scale bar, 5 μm.

Figure 2-3

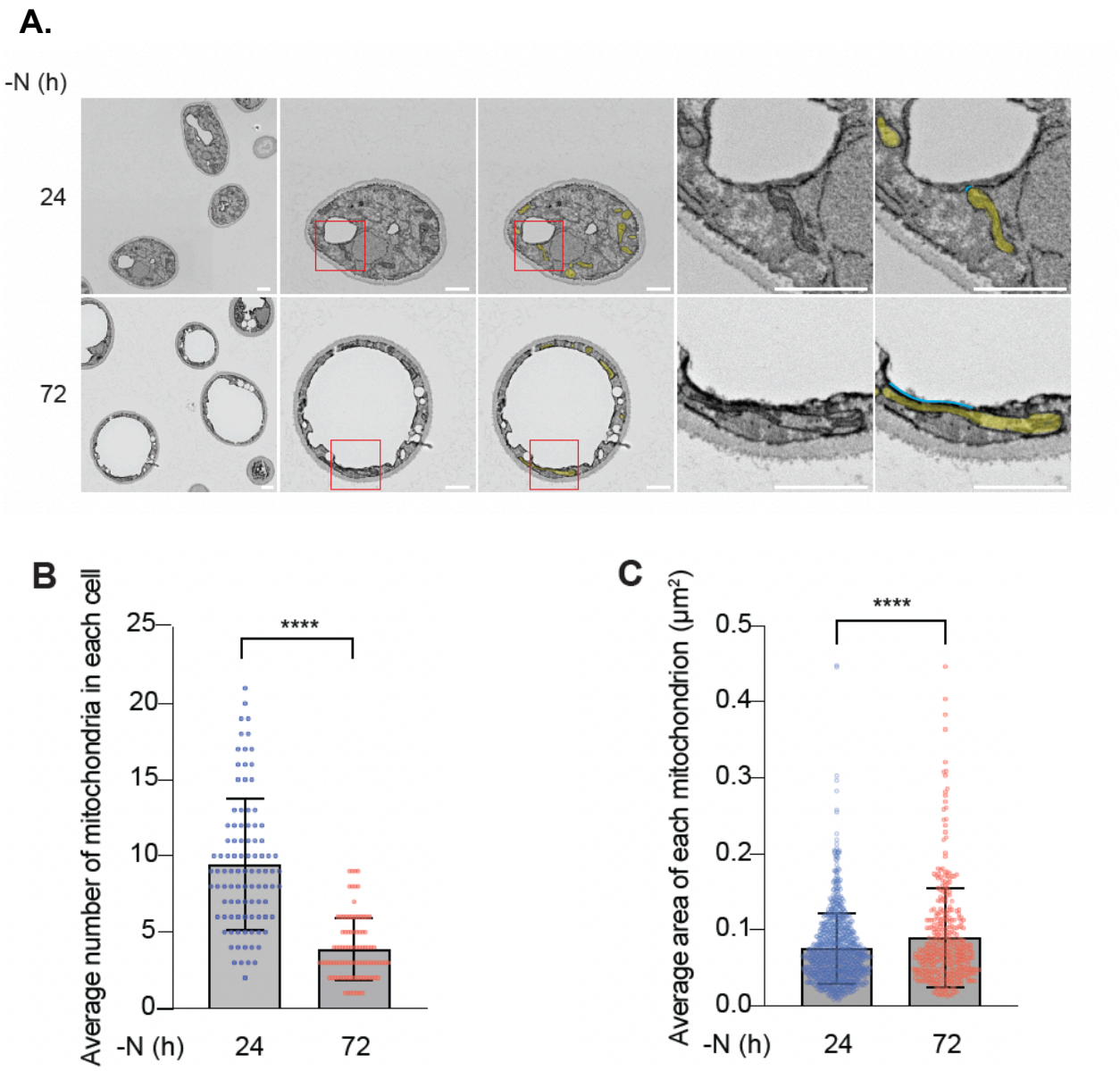

Figure 2-3. *L. starkeyi* cells under prolonged nitrogen starvation contain elongated mitochondria in close proximity to a giant LD. (A) Cells were grown under nitrogen starvation (-N) for 24 h and 72 h. Mitochondrial morphology was observed by SEM at the indicated time points. Mitochondria were depicted in yellow color. Around 100 cells for each time point were counted to quantify mitochondrial number (B), and size (C). Scale bar, 1 μm.

Figure 2-3

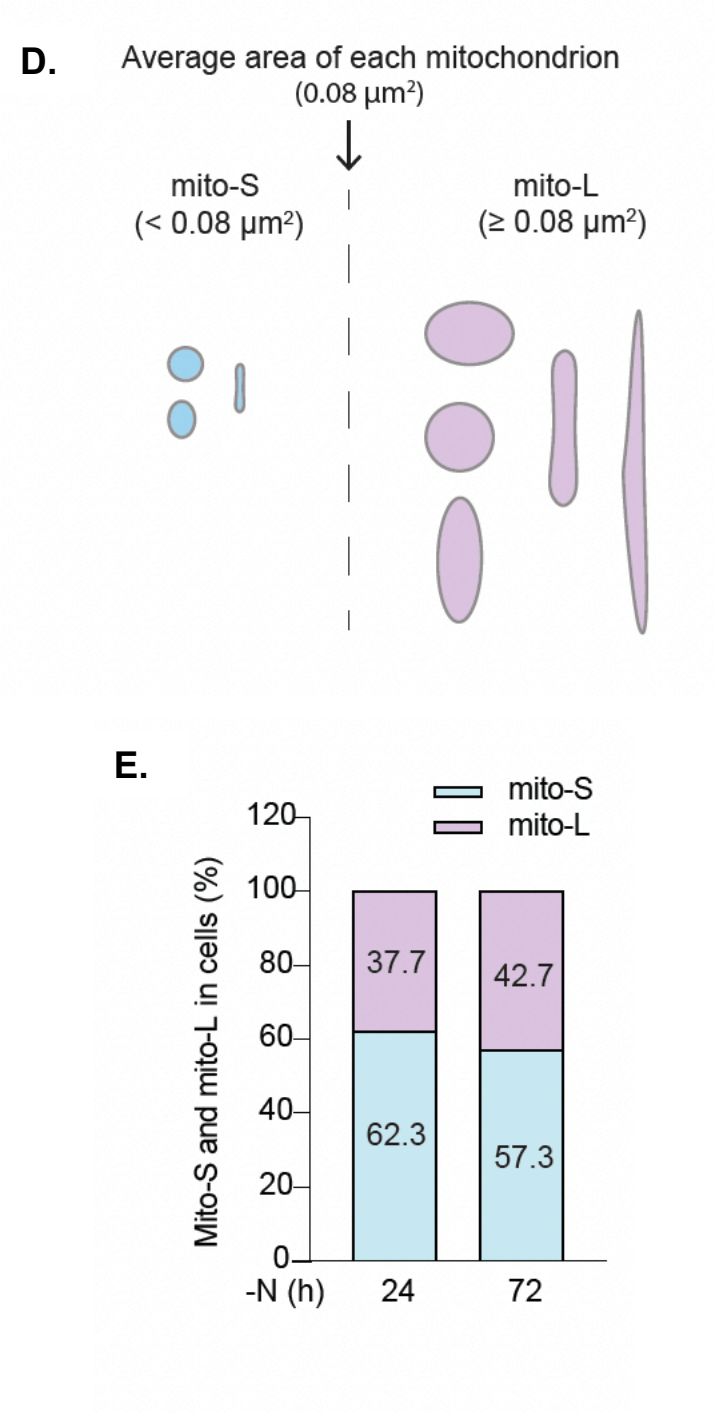

Figure 2-3. Classification of mitochondria in nitrogen-depleted *L. starkeyi* cells. (D) A scheme to categorize mitochondria into small-sized (mito-S) and large-sized (mito-L) mitochondria groups by the average size of a single mitochondrion (≈ 0.08 μm2) as a thresh hold. (E) All the mitochondria in around 100 cells were classified into mito-S and mito-L, and their percentage was calculated.

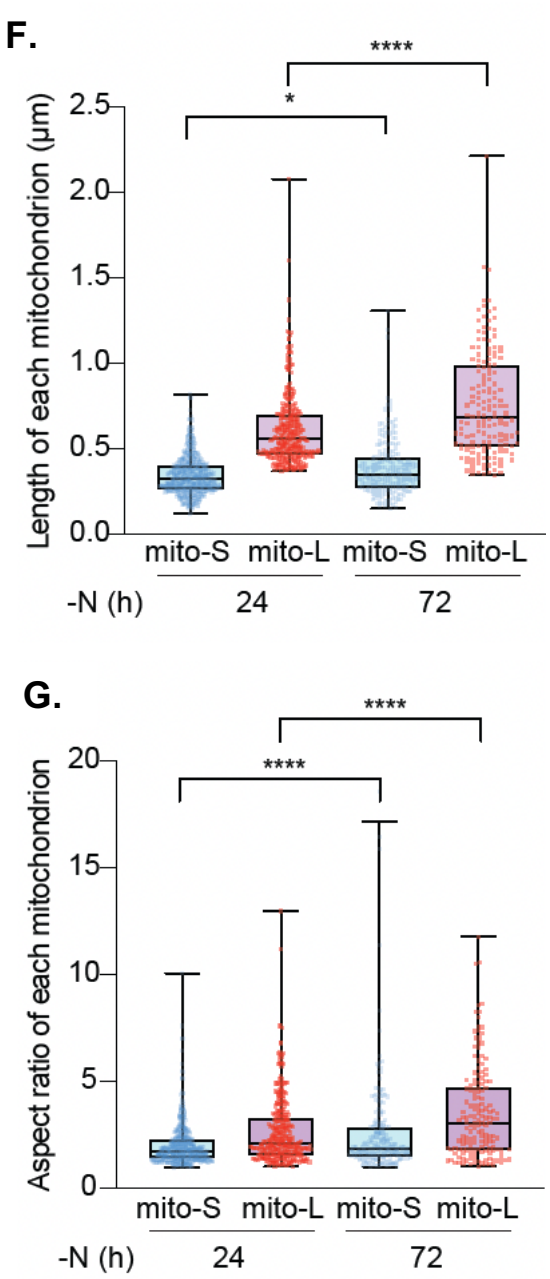

Figure 2-3. *L. starkeyi* cells under prolonged nitrogen starvation contain elongated mitochondria in close proximity to a giant LD. The length (F) and aspect ratio (G) of small-sized mitochondria (mito-S) and large-sized mitochondria (mito-L) were measured using Image J software (NIH Image J system, Bethesda, MD, USA). Around 100 cells with LDs were counted to analyze the percentage of cells with mitochondria-LD proximity (H), and the length of mitochondria-LD proximity (I). Scale bar, 1 μm.

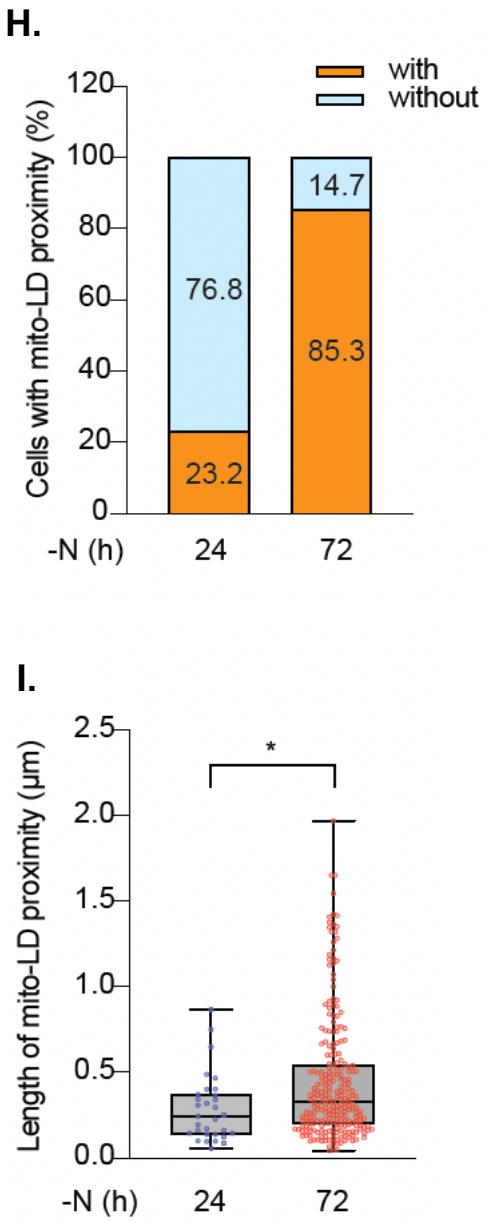

Figure 2-3. *L. starkeyi* cells under prolonged nitrogen starvation contain elongated mitochondria in close proximity to a giant LD. The length (F) and aspect ratio (G) of small-sized mitochondria (mito-S) and large-sized mitochondria (mito-L) were measured using Image J software (NIH Image J system, Bethesda, MD, USA). Around 100 cells with LDs were counted to analyze the percentage of cells with mitochondria-LD proximity (H), and the length of mitochondria-LD proximity (I). Scale bar, 1 µm.

Figure 2-4

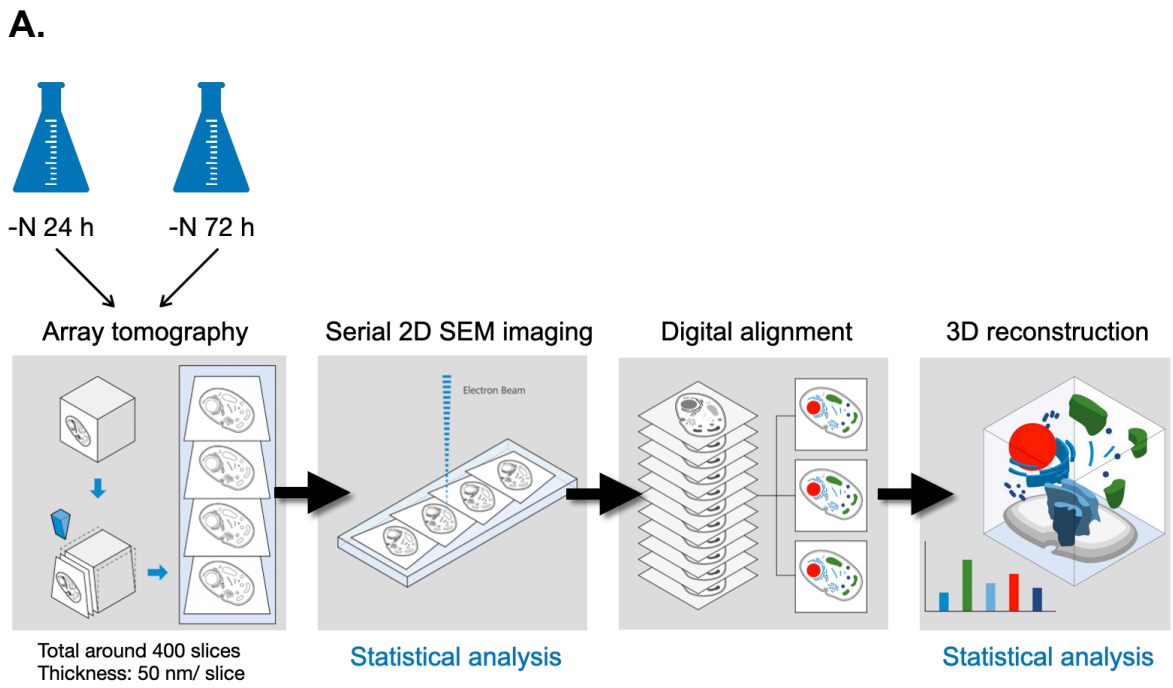

Figure 2-4. Mitochondria form tubules and sheets closely juxtaposed to a giant LD in nitrogen-depleted *L. starkeyi* cells. Cells grown under nitrogen starvation (-N) for 24 h and 72 h were subjected to chemical fixation, embedded in a resin, cut into an array of ultrathin sections, imaged with SEM (A), and reconstituted into a 3D data set (B). The number indicated in the black box in each image is the order of sections for cells grown for the indicated time points. Mitochondria were depicted in yellow color. The 3D reconstruction of mitochondria and LDs was performed using AMIRA 3D 2022.2. Scale bar, 1μm.

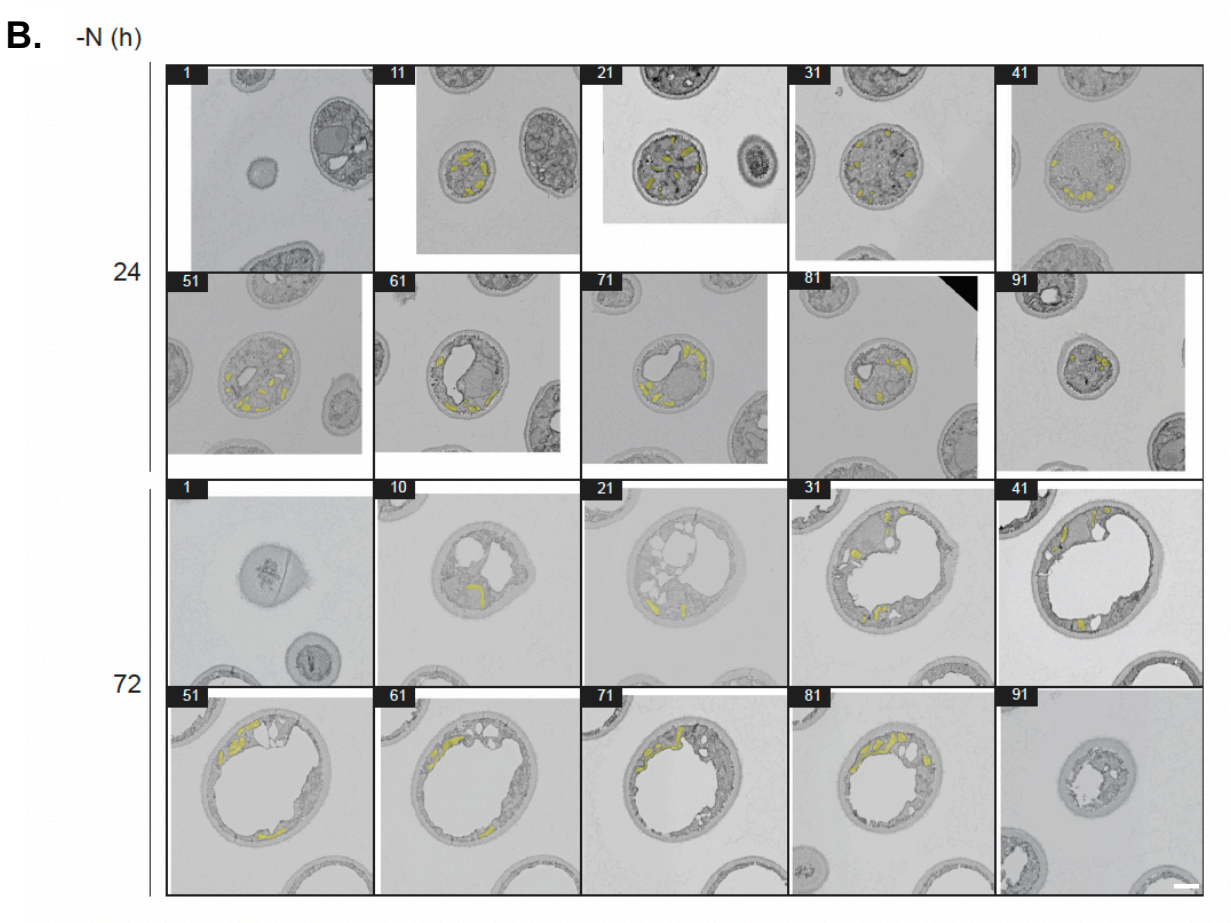

Figure 2-4. Mitochondria form tubules and sheets closely juxtaposed to a giant LD in nitrogen-depleted *L. starkeyi* cells. Cells grown under nitrogen starvation (-N) for 24 h and 72 h were subjected to chemical fixation, embedded in a resin, cut into an array of ultrathin sections, imaged with SEM (A and B), and reconstituted into a 3D data set (C). The number indicated in the black box in each image is the order of sections for cells grown for the indicated time points. Mitochondria were depicted in yellow color. The 3D reconstruction of mitochondria and LDs was performed using AMIRA 3D 2022.2. Scale bar, 1μm.

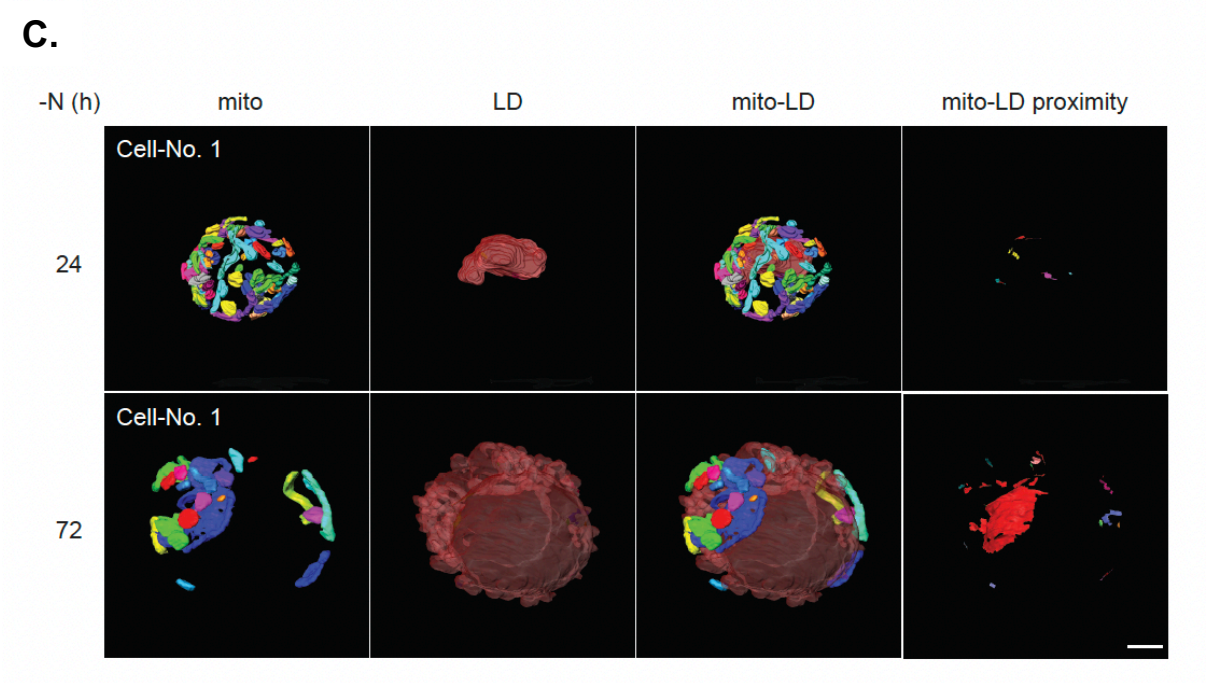

Figure 2-4. Mitochondria form tubules and sheets closely juxtaposed to a giant LD in nitrogen-depleted *L. starkeyi* cells. Cells grown under nitrogen starvation (-N) for 24 h and 72 h were subjected to chemical fixation, embedded in a resin, cut into an array of ultrathin sections, imaged with SEM (A and B), and reconstituted into a 3D data set (C). The number indicated in the black box in each image is the order of sections for cells grown for the indicated time points. Mitochondria were depicted in yellow color. The 3D reconstruction of mitochondria and LDs was performed using AMIRA 3D 2022.2. Scale bar, 1μm.

Figure 2-5

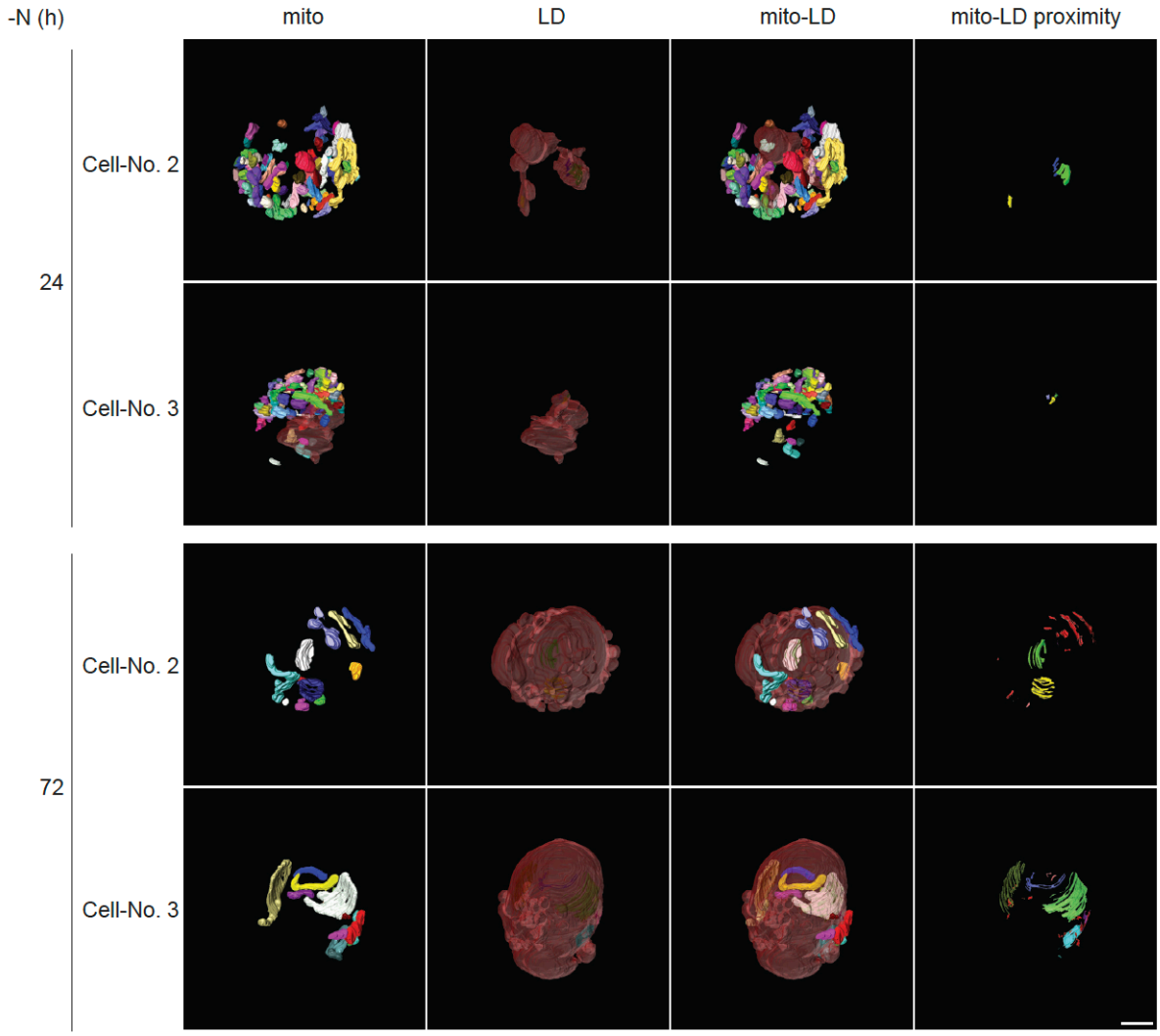

Figure 2-5. Mitochondria form tubules and sheets in close proximity to a giant LD in *L. starkeyi* cells under nitrogen starvation. Cells grown under nitrogen starvation (-N) for 24 h and 72 h were subjected to chemical fixation, embedded in a resin, cut into an array of ultrathin sections, imaged with SEM, and reconstituted into a 3D data set using Amira 3D 2022.2. Scale bar, 1μm.

Figure 2-6

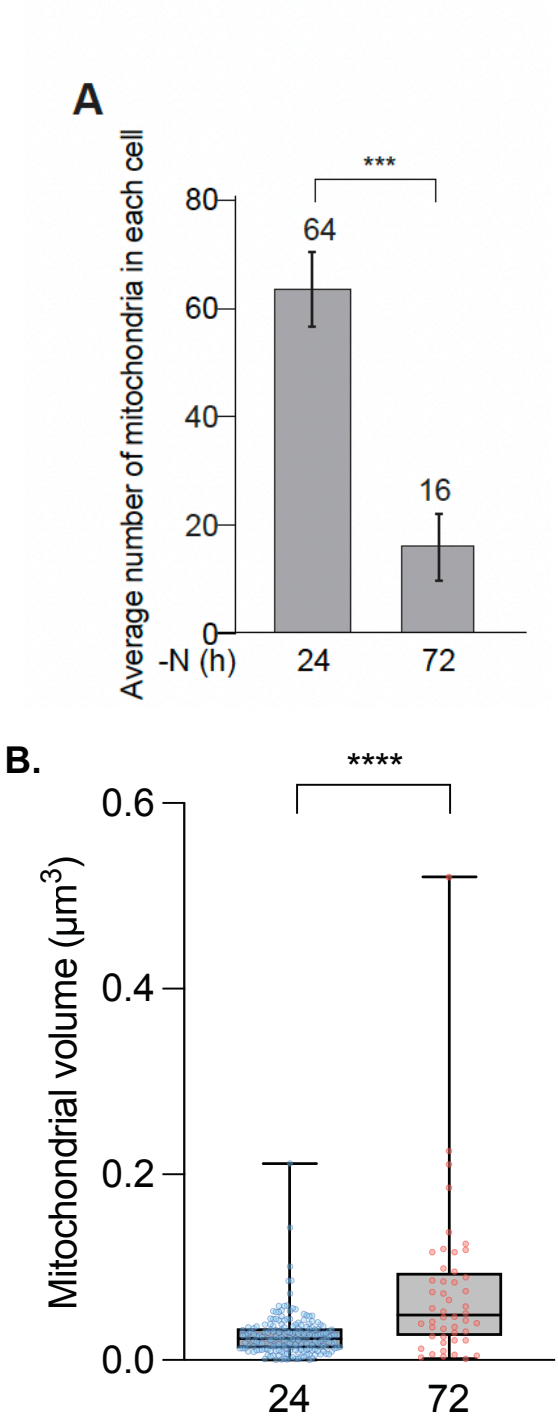

Figure 2-6. Mitochondria change in smaller number, higher volume, and bigger LD-proximity during LD expansion in nitrogen-depleted *L. starkeyi* cells. The average number of mitochondria in each cell (A), volume of each mitochondrion (B), percentage of mitochondria in close proximity to LDs (C), and average total area of mito-LD proximity in each cell (D) were quantified with the 3D-reconstituted dataset for three cells.

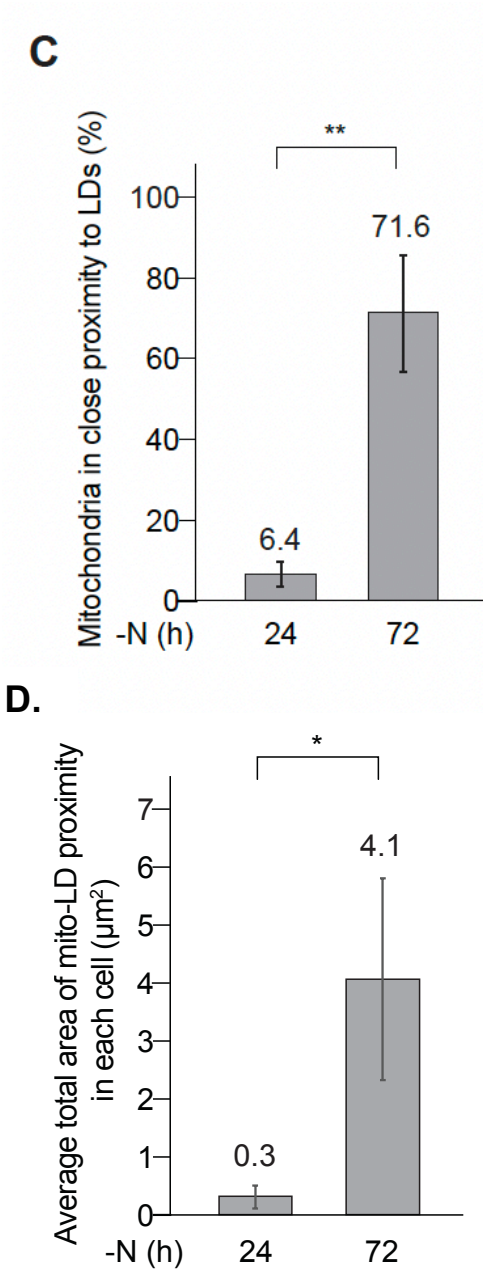

Figure 2-6. Mitochondria change in smaller number, higher volume, and bigger LD-proximity during LD expansion in nitrogen-depleted *L. starkeyi* cells. The average number of mitochondria in each cell (A), volume of each mitochondrion (B), percentage of mitochondria in close proximity to LDs (C), and average total area of mito-LD proximity in each cell (D) were quantified with the 3D-reconstituted dataset for three cells.

E.

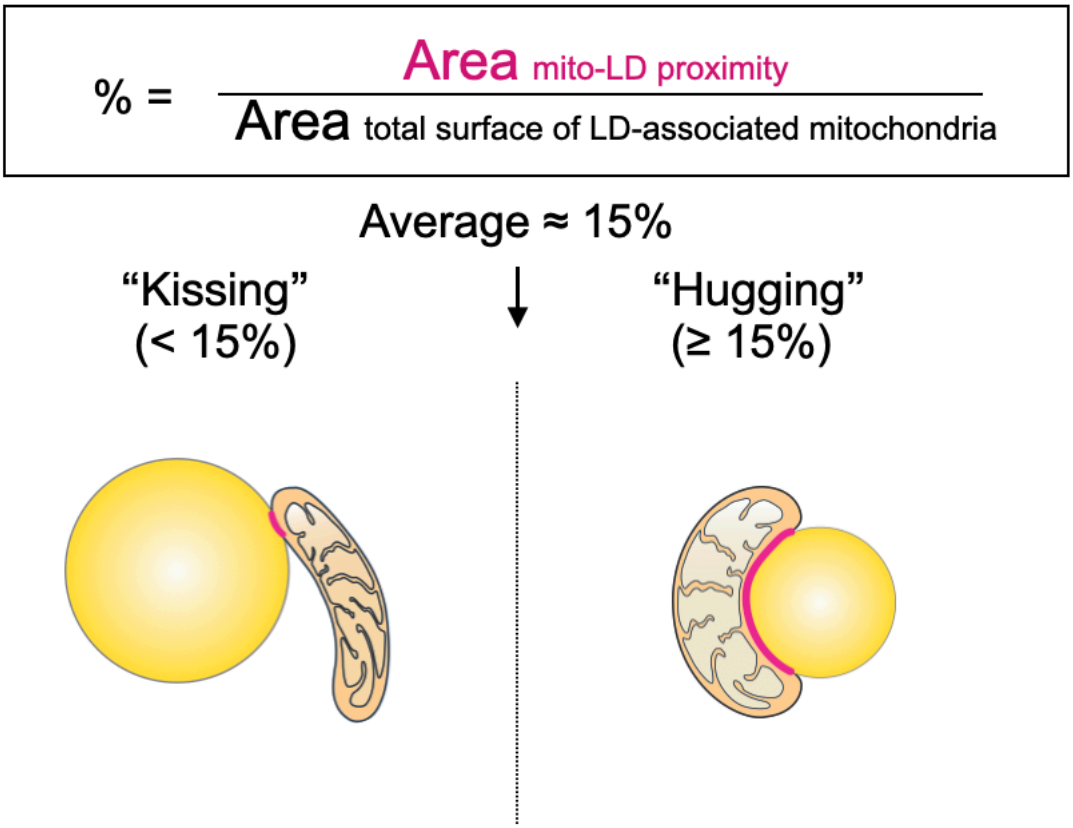

Figure 2-6. Mitochondria change in smaller number, higher volume, and bigger LD-proximity during LD expansion in nitrogen-depleted *L. starkeyi* cells. (E) A scheme to categorize LD-mitochondria proximity into "Kissing" and "Hugging" groups by the average percentage of mito-LD proximity area to the total area of each LD-associated mitochondrion (≈ 15%) as a threshold.

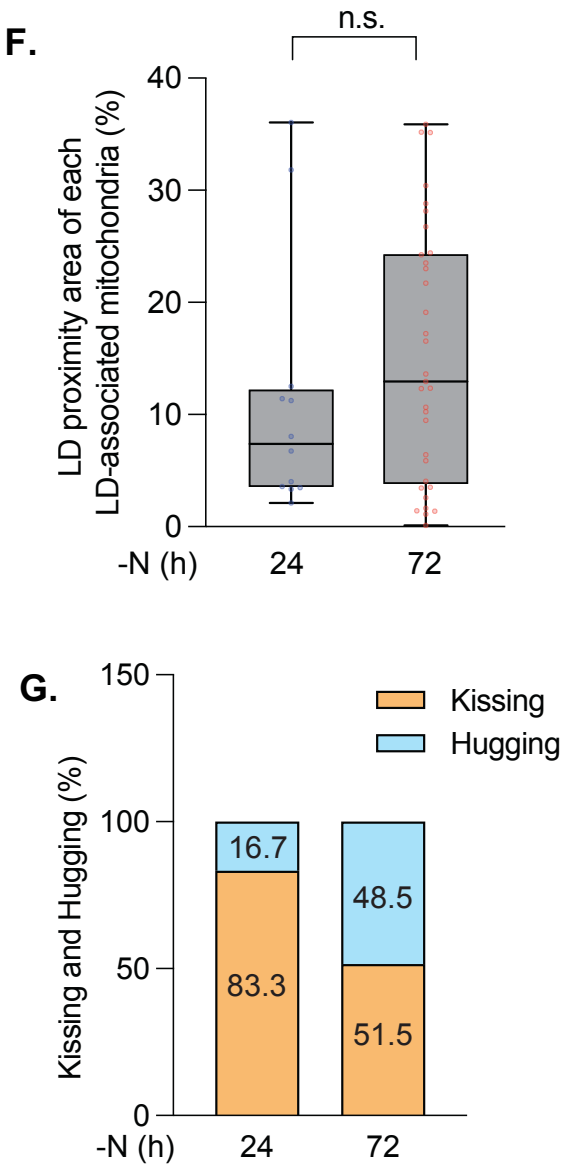

Figure 2-6. Mitochondria change in smaller number, higher volume, and bigger LD-proximity during LD expansion in nitrogen-depleted *L. starkeyi* cells. (E) A scheme to categorize LD-mitochondria proximity into "Kissing" and "Hugging" groups by the average percentage of mito-LD proximity area to the total area of each LD-associated mitochondrion (≈ 15%) as a threshold. (F) The percentage of LD proximity area of each LD-associated mitochondria (%) and (G) the percentage of Kissing and Hugging contact with the 3D-reconstituted dataset for three cells.

Figure 2-7

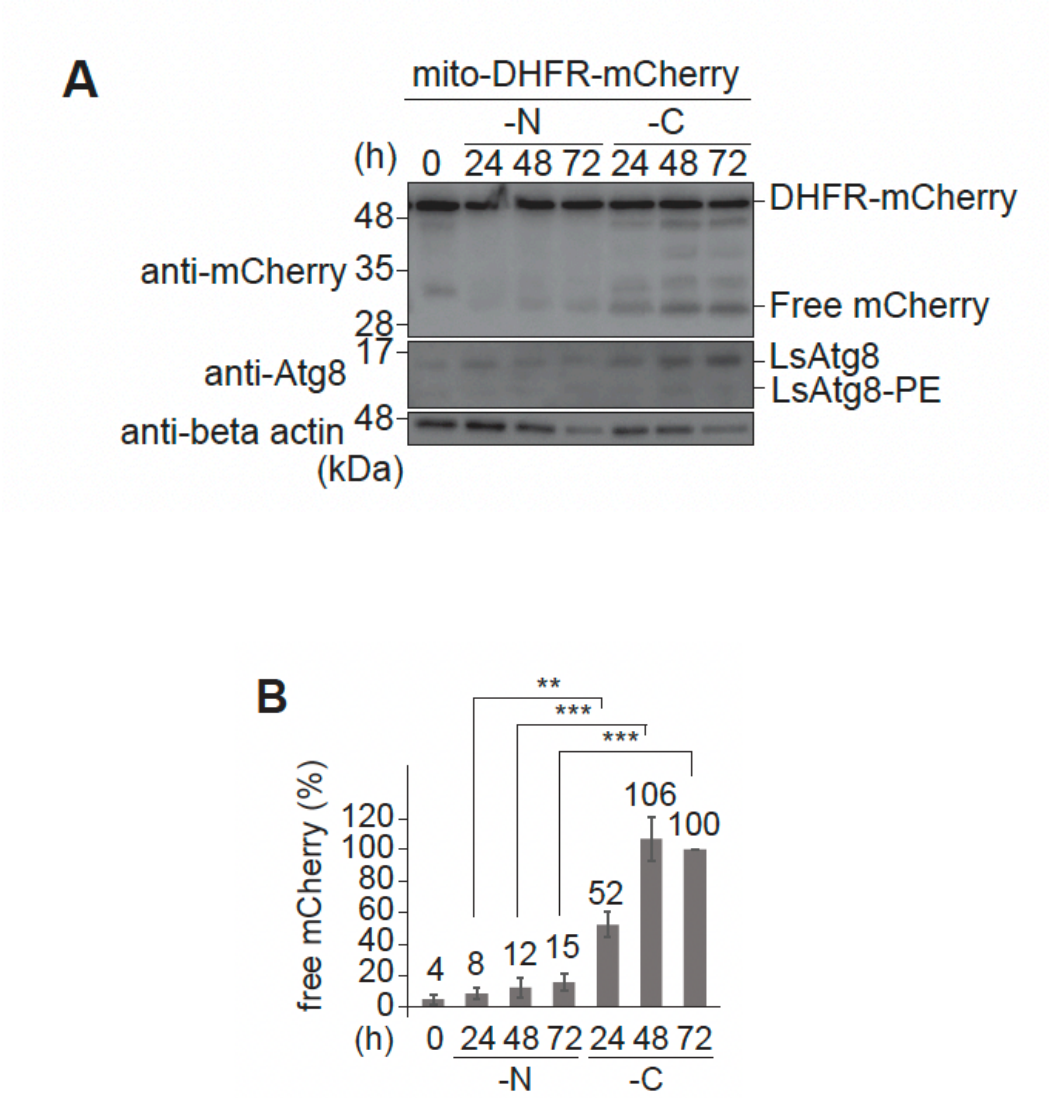

Figure 2-7. *L. starkeyi* cells under nitrogen starvation exhibit strong suppression of mitochondrial degradation and autophagy. Cells expressing mito-DHFR-mCherry (A) or mCherry-LsAtg8 (C) were grown under nitrogen (-N) or carbon (-C) starvation, collected at the indicated time points, and subjected to western blotting. Free mCherry signals derived from (A) or (C) were quantified more than three times in independent experiments as shown in (B) or (D), respectively. The signal intensity of free mCherry in carbon-depleted cells at the 72 h time point was set to 100%. Data represent the averages of all experiments, with bars indicating standard deviations. Protein signals generated from intracellular cleavage of mCherry-LsAtg8 are indicated with arrowheads. The anti-Atg8 antibody for *S. cerevisiae* was used to detect free and lipidated LsAtg8. The beta actin was monitored as a loading control.

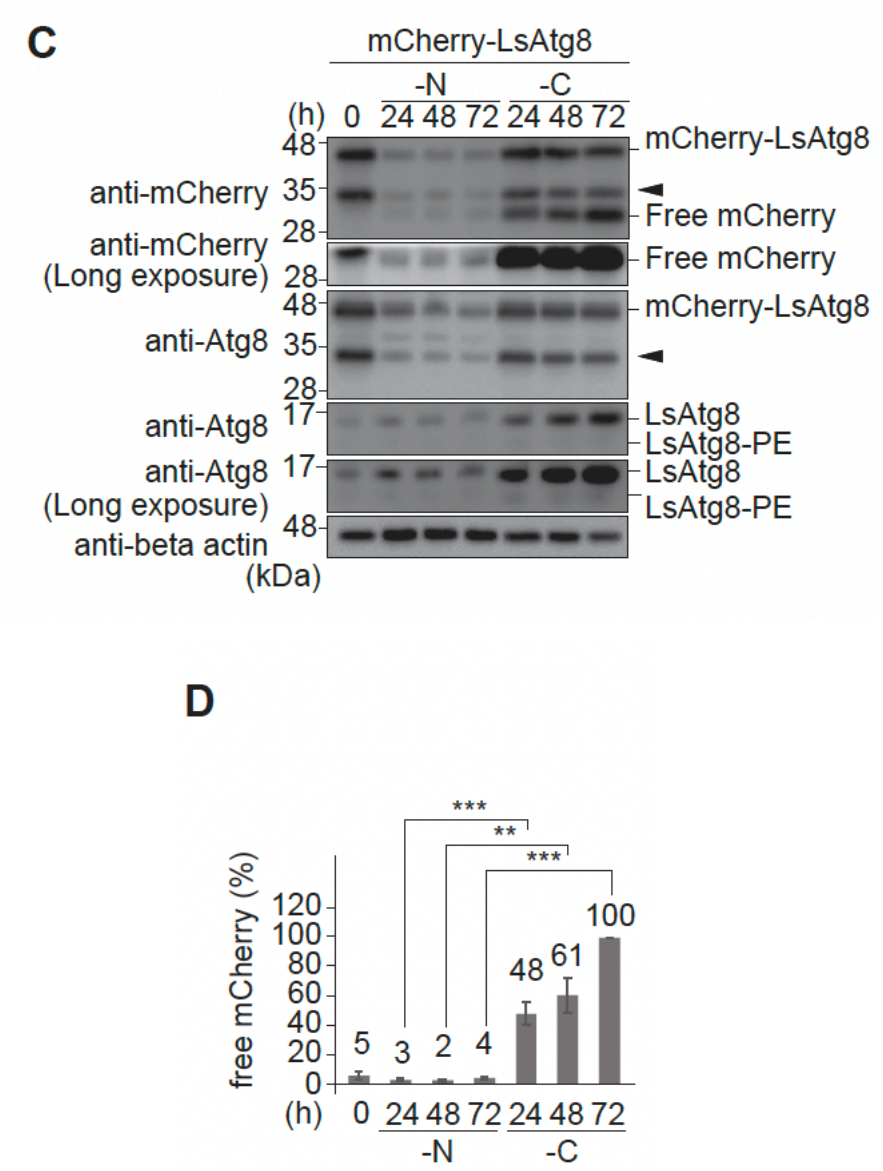

Figure 2-7. *L. starkeyi* cells under nitrogen starvation exhibit strong suppression of mitochondrial degradation and autophagy. Cells expressing mito-DHFR-mCherry (A) or mCherry-LsAtg8 (C) were grown under nitrogen (-N) or carbon (-C) starvation, collected at the indicated time points, and subjected to western blotting. Free mCherry signals derived from (A) or (C) were quantified more than three times in independent experiments as shown in (B) or (D), respectively. The signal intensity of free mCherry in carbon-depleted cells at the 72 h time point was set to 100%. Data represent the averages of all experiments, with bars indicating standard deviations. Protein signals generated from intracellular cleavage of mCherry-LsAtg8 are indicated with arrowheads. The anti-Atg8 antibody for *S. cerevisiae* was used to detect free and lipidated LsAtg8. The beta actin was monitored as a loading control.

Figure 2-8

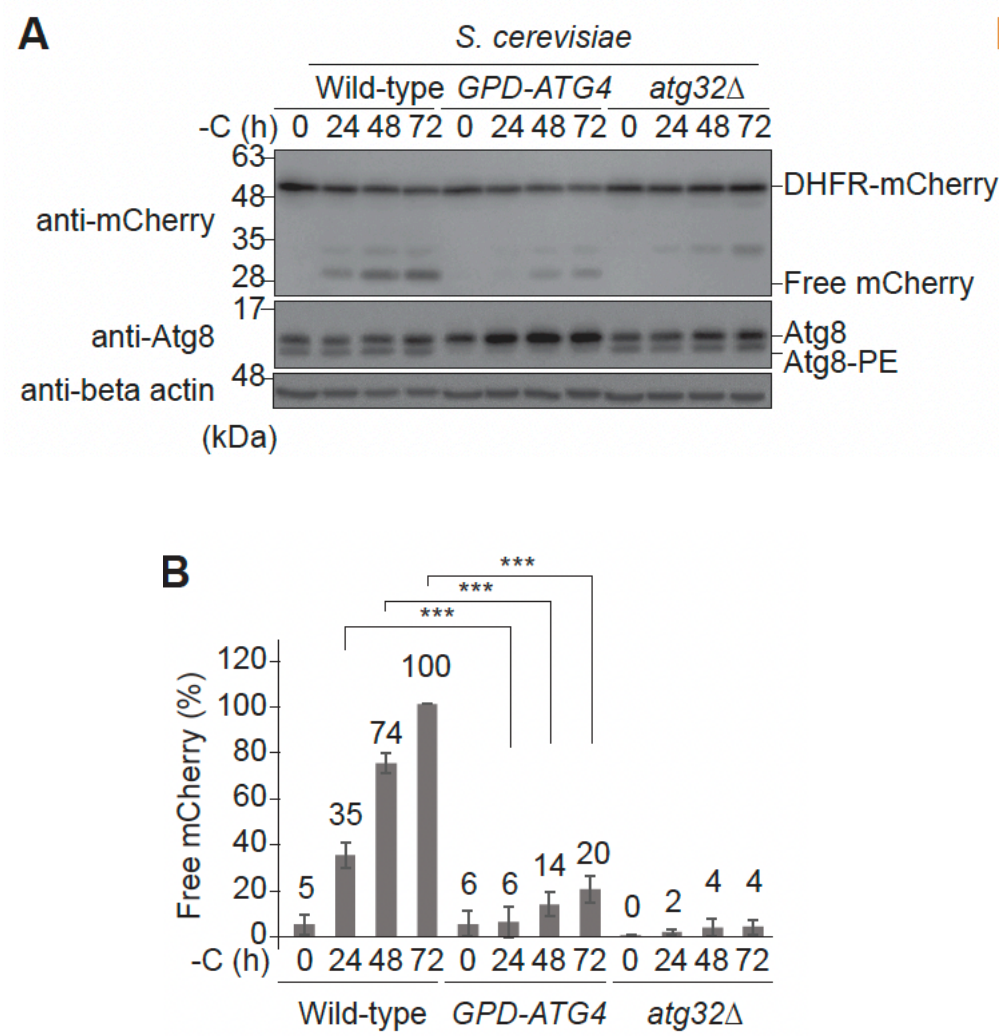

Figure 2-8. Overexpression of Atg4 leads to a strong reduction in mitophagy and autophagy in *S. cerevisiae* cells under carbon starvation. Wild-type and Atg4-overexpressing (*GPD-ATG4*) cells were grown under carbon starvation (-C), collected at the indicated time points, and subjected to western blotting. These strains are derivatives expressing mito-DHFR-mCherry or Tdh3-mCherry for monitoring mitophagy (A and B) or autophagy (C and D), respectively. Cells lacking Atg32 (atg32D) or Atg7 (atg7D) were used as a negative control for mitophagy or autophagy, respectively. Free mCherry signals were quantified more than three times in independent experiments as shown in (B and D). The signal intensity of free mCherry in wild-type cells at the 72 h time point was set to 100%. Data represent the averages of all experiments, with bars indicating standard deviations. The beta actin was monitored as a loading control.

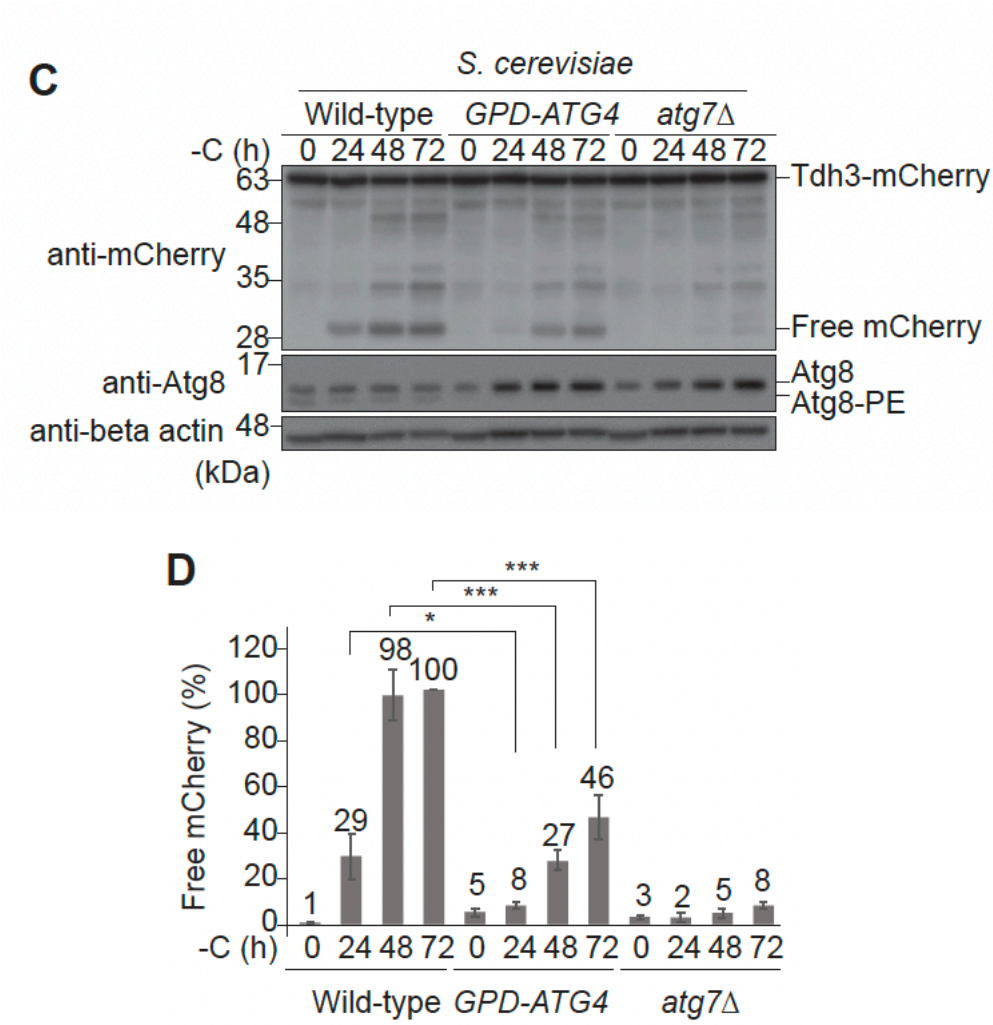

Figure 2-8. Overexpression of Atg4 leads to a strong reduction in mitophagy and autophagy in *S. cerevisiae* cells under carbon starvation. Wild-type and Atg4-overexpressing (*GPD-ATG4*) cells were grown under carbon starvation (-C), collected at the indicated time points, and subjected to western blotting. These strains are derivatives expressing mito-DHFR-mCherry or Tdh3-mCherry for monitoring mitophagy (A and B) or autophagy (C and D), respectively. Cells lacking Atg32 (atg32D) or Atg7 (atg7D) were used as a negative control for mitophagy or autophagy, respectively. Free mCherry signals were quantified more than three times in independent experiments as shown in (B and D). The signal intensity of free mCherry in wild-type cells at the 72 h time point was set to 100%. Data represent the averages of all experiments, with bars indicating standard deviations. The beta actin was monitored as a loading control.

Figure 2-9

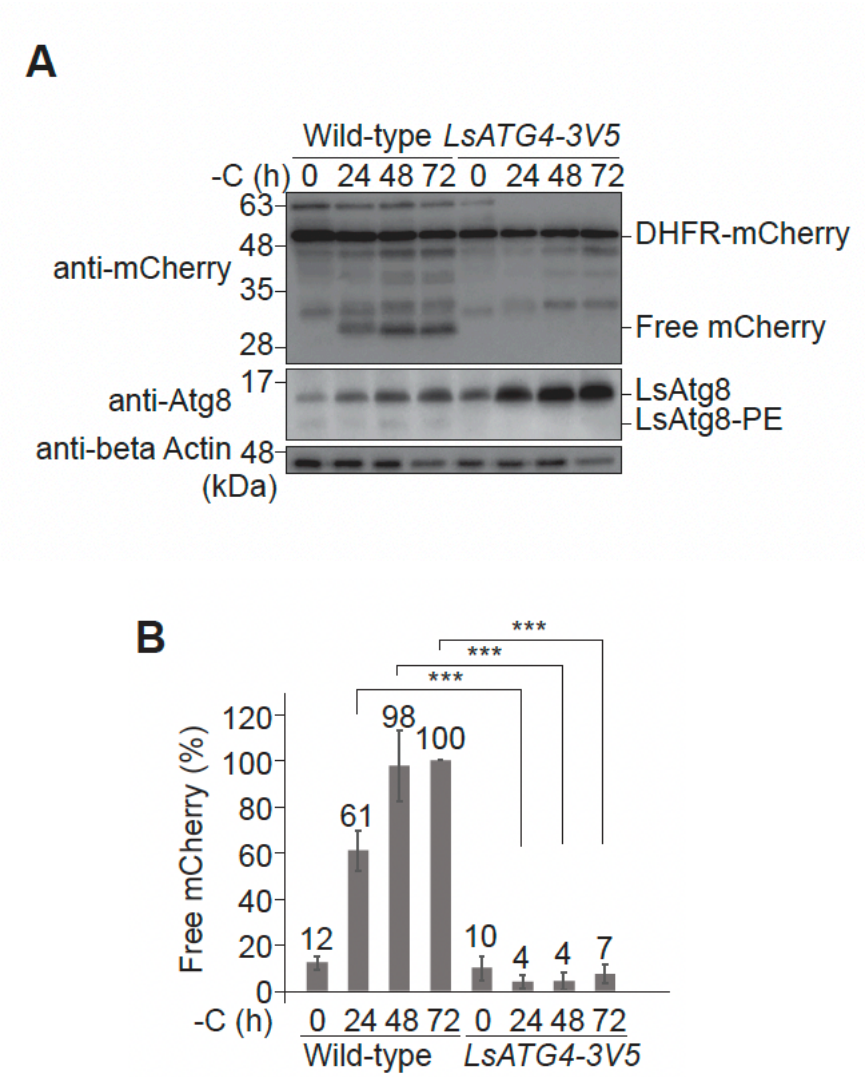

Figure 2-9. Overexpression of LsAtg4 leads to a strong reduction in mitochondrial degradation in *L. starkeyi* cells under carbon starvation. Wild-type and LsAtg4-overexpressing (*LsATG4-3V5*) cells were grown under carbon starvation (-C), collected at the indicated time points, and subjected to western blotting (A). These strains are derivatives expressing mito-DHFR-mCherry. Free mCherry signals were quantified more than three times in independent experiments as shown in (B). The signal intensity of free mCherry in wild-type cells at the 72 h time point was set to 100%. Data represent the averages of all experiments, with bars indicating standard deviations. The anti-Atg8 antibody for *S. cerevisiae* was used to detect free and lipidated LsAtg8. The beta actin was monitored as a loading control.

Figure 2-10

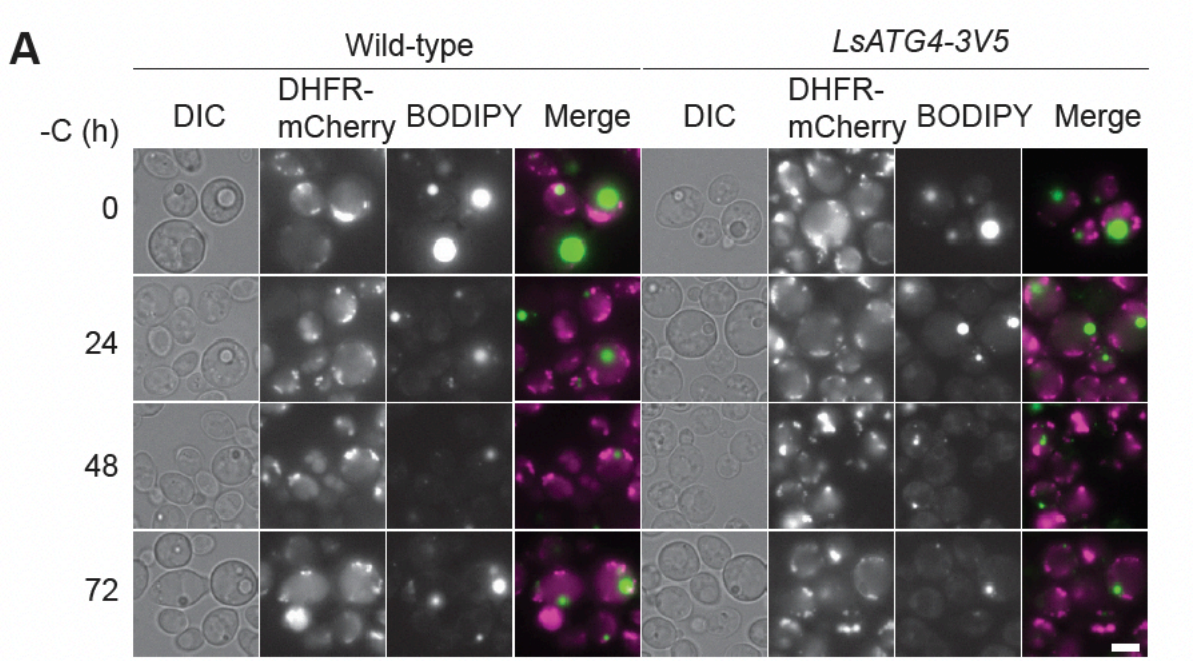

Figure 2-10. LD expansion is not promoted in carbon-depleted *L. starkeyi* cells overexpressing LsAtg4. Wild-type and LsAtg4-overexpressing (*LsATG4-3V5*) cells were grown under carbon starvation (-C), collected at the indicated time points, and subjected to fluorescence microscopy (A). These strains are derivatives expressing mito-DHFR-mCherry. Scale bar, 5 μm. The average total area (B) and number (C) of LDs in each cell were quantified by the area of BODIPY signals. The average area (D) of each mitochondrion and average number (E) of mitochondria in each cell were quantified by the area of mCherry signals.

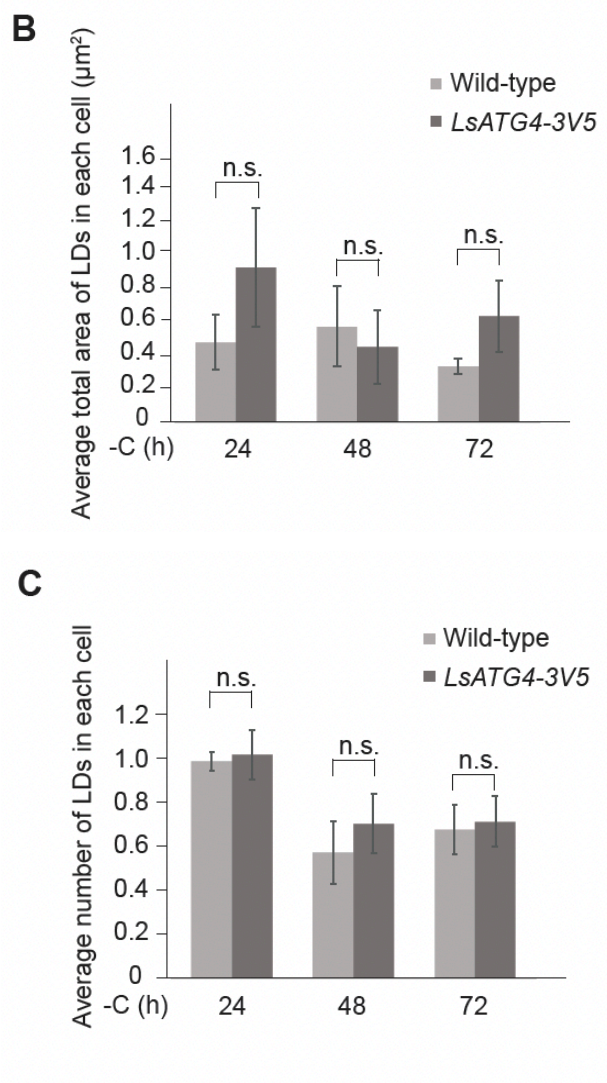

Figure 2-10. LD expansion is not promoted in carbon-depleted *L. starkeyi* cells overexpressing LsAtg4. Wild-type and LsAtg4-overexpressing (*LsATG4-3V5*) cells were grown under carbon starvation (-C), collected at the indicated time points, and subjected to fluorescence microscopy (A). These strains are derivatives expressing mito-DHFR-mCherry. Scale bar, 5 μm. The average total area (B) and number (C) of LDs in each cell were quantified by the area of BODIPY signals. The average area (D) of each mitochondrion and average number (E) of mitochondria in each cell were quantified by the area of mCherry signals.

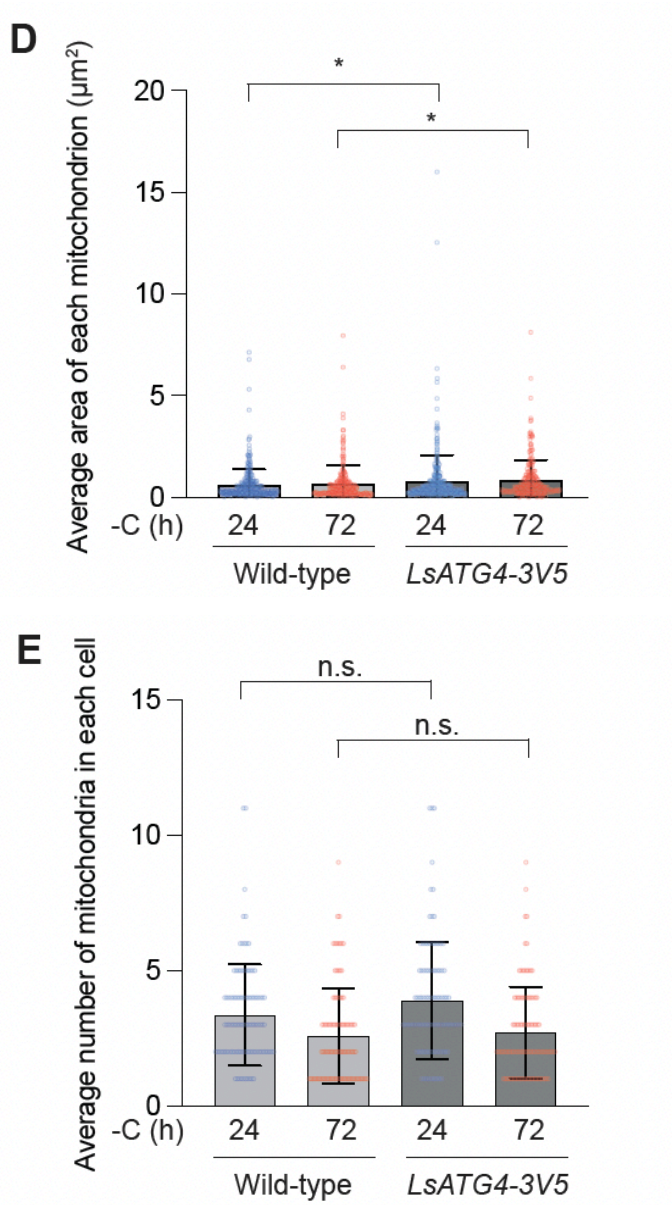

Figure 2-10. LD expansion is not promoted in carbon-depleted *L. starkeyi* cells overexpressing LsAtg4. Wild-type and LsAtg4-overexpressing (*LsATG4-3V5*) cells were grown under carbon starvation (-C), collected at the indicated time points, and subjected to fluorescence microscopy (A). These strains are derivatives expressing mito-DHFR-mCherry. Scale bar, 5 μm. The average total area (B) and number (C) of LDs in each cell were quantified by the area of BODIPY signals. The average area (D) of each mitochondrion and average number (E) of mitochondria in each cell were quantified by the area of mCherry signals.

Figure 2-11

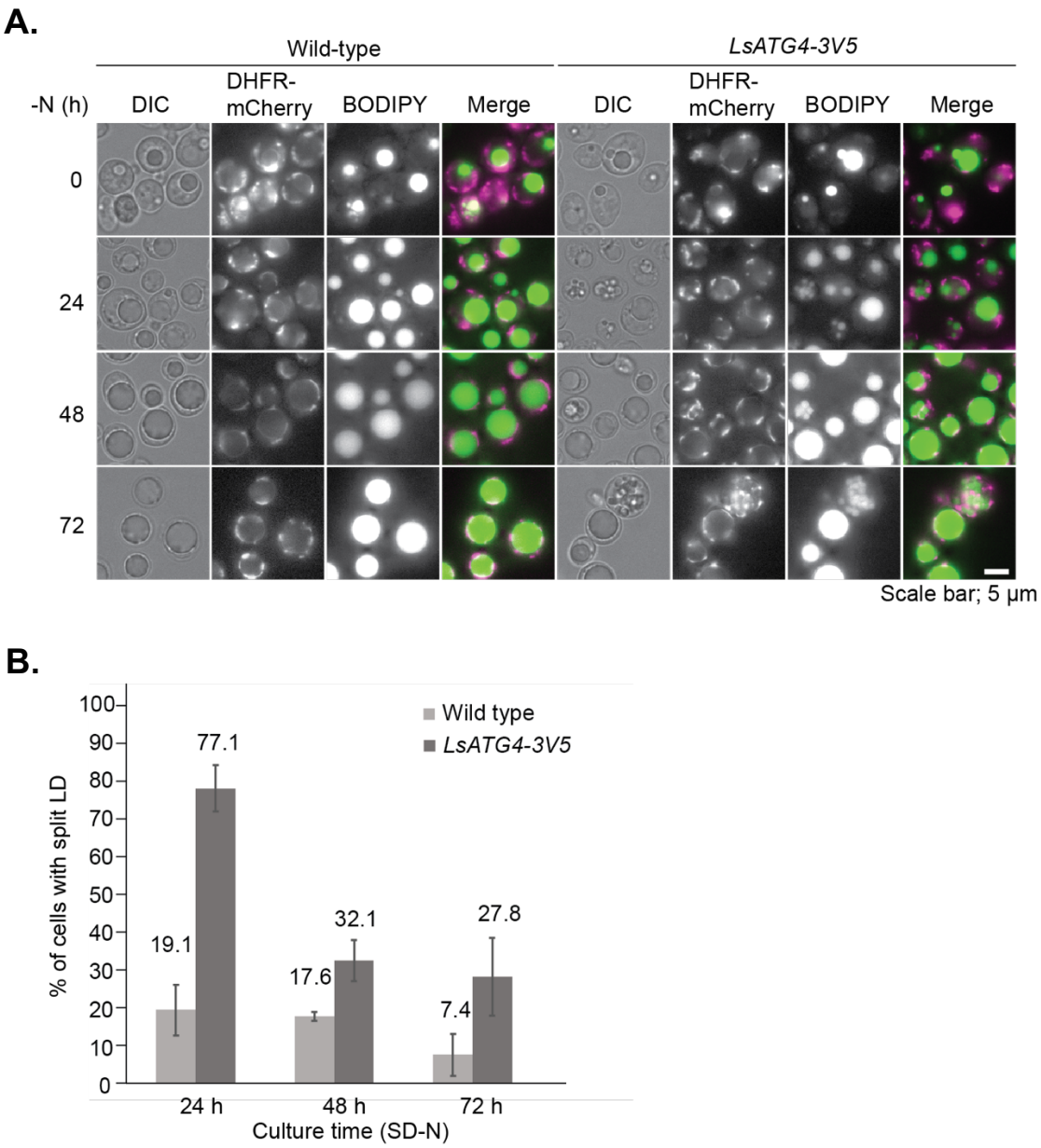

Figure 2-11. LD integrity was disrupted by over-expression of *LsATG4* in *L. starkeyi* cells under nitrogen starvation. Mito-DHFR-mCherry expressing wild-type and *LsATG4*-overexpressing *L. starkeyi* cells were cultured under -N condition. The mitochondrial shape (a) and the percentage of cells with split LDs (b) were analyzed at the indicated time points using a fluorescence microscope. BODIPY staining was used to observe and quantify LDs.

Figure 2-12

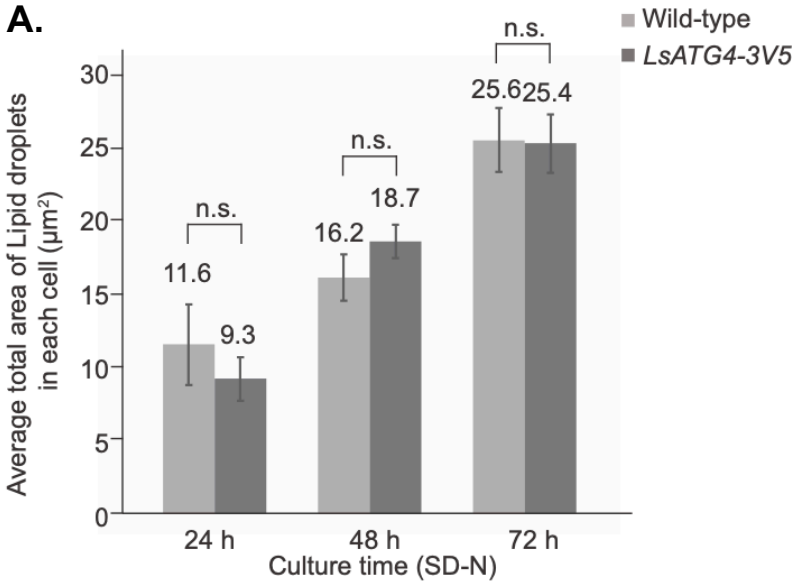

Figure 2-12. LD integrity was disrupted by over-expression of *LsATG4* in *L. starkeyi* cells under nitrogen starvation. Mito-DHFR-mCherry expressing wild-type and *LsATG4*-overexpressing *L. starkeyi* cells were cultured under -N condition. (A) Average total area of Lipid droplets in each cell were analyzed at the indicated time points using a fluorescence microscope. BODIPY staining was used to observe and quantify LDs.

5. Acknowledgments

First, I would like to express my gratitude to Prof. Koji Okamoto for supporting me in my research study and my life.

I would also like to thank Prof. Yuko Takayama (Teikyo University, Japan) for transformation reagents and protocols, Prof. Hiroaki Takaku (Niigata University of Pharmacy and Applied Life Sciences, Japan) for the plasmid pKS-18S-hph, Prof. Keisuke Ohta (Kurume University, Japan) for supporting EM observation, Prof. Wei Fanyan (Tohoku University, Japan) for modomics analysis, Prof. Yuhei Araiso (Kanazawa University, Japan) for mitochondrial membrane preparation, Prof. Hidetaka Kosako (Tokushima University, Japan) for ubiquitinylated protein analysis.

I'm also very appreciative to all the members of the Laboratory of Mitochondrial Dynamics (Mitsutaka Kubota, Yuki Nakayama, Sayaka Nagano, Sato Rio, Peijin Li, Qiao Liu and Yuko Imada) and former lab members (Mashun Onishi, Schuster Ramona, Yang Liu, Yuan Tian, Ziyi Wang, Kanako Fujii, Ritsu Shibata, Shiori Yuki, Yukiko Omi) for helpful discussions and.

I am also very grateful to Prof. Fumiyo Ikeda, Prof. Takeshi Noda and Prof. Tatsuo Fukagawa for kindly serving as committee members of my PhD defense.

Finally, I would like to thank my parents (Yiming Duan and Xuezhi Kang) for supporting my research life at Osaka University and thank myself for all the efforts I have made in these five years.

6. Research Achievement

Publications

1. **Duan, L.**, Tougo, A., Ohta, K. and Okamoto, K. Mitochondria-giant lipid droplet proximity and autophagy suppression in nitrogen-depleted oleaginous yeast *Lipomyces starkeyi* cells. *J. Biochem.*, **in press**. https://doi.org/10.1093/jb/mvae069

2. **Duan, L.** and Okamoto, K. (2021). Mitochondrial dynamics and degradation in the oleaginous yeast *Lipomyces starkeyi*. *Genes Cells*, 26(8), 627–635.

3. Onishi, M., Kubota, M., **Duan, L.**, Tian, Y. and Okamoto, K. (2023). The GET pathway serves to activate Atg32-mediated mitophagy by ER targeting of the Ppg1-Far complex. *Life Sci. Alliance*, 6(4), e202201640

Conference Presentations

Oral presentations

1. **Duan L.** and Okamoto K.
Mitochondrial shaping and degradation in the oleaginous yeast *Lipomyces starkeyi*
The 67th The Japanese Biochemical Society, Kinki Branch
No. ET156, online, May, 2021

Poster Presentations

2. **Duan L.** and Okamoto K.
Label-free photothermal microscopy imaging of mitochondria in the oleaginous yeast *Lipomyces starkeyi*
The 43rd Annual Meeting of the Molecular Biology Society of Japan
No. 3LBA-075, Online, December, 2020

3. **Duan, L.,** Araiso, Y., Kosako, H., and Okamoto K.
Exploring mitophagy-related factors in the oleaginous yeast *Lipomyces starkeyi* using AirID, a new enzyme for proximity biotinylation
The 45th Annual Meeting of the Molecular Biology Society of Japan
No. 2P-266, on site, December, 2022

4. **Duan L.** and Okamoto K.
Mitochondrial degradation and lipid droplet formation in the oleaginous yeast *Lipomyces starkeyi*

The 46th Annual Meeting of the Molecular Biology Society of Japan

No. 1P-420, on site, December, 2023

Grants and scholarships

1. JST SPRING Fellowship

October 1, 2021 - November 30, 2024